EXTINGUISHMENT OF A SOLID ROCKET MOTOR BY RAPID DEPRESSURIZATION AFTER NOZZLE DETACHMENT

A THESIS SUBMITTED TO
THE GRADUATE SCHOOL OF NATURAL AND APPLIED SCIENCES
OF
MIDDLE EAST TECHNICAL UNIVERSITY

BY

RÜŞTÜ GÖRKEM YILMAZ

IN PARTIAL FULFILLMENT OF THE REQUIREMENTS
FOR
THE DEGREE OF MASTER OF SCIENCE
IN
AEROSPACE ENGINEERING

JANUARY 2023

Approval of the thesis:

EXTINGUISHMENT OF A SOLID ROCKET MOTOR BY RAPID DEPRESSURIZATION AFTER NOZZLE DETACHMENT

submitted by **RÜŞTÜ GÖRKEM YILMAZ** in partial fulfillment of the requirements for the degree of **Master of Science** i**n Aerospace Engineering, Middle East Technical University** by,

Prof. Dr. Halil Kalıpçılar
Dean, Graduate School of **Natural and Applied Sciences** _____

Prof. Dr. Serkan Özgen
Head of the Department, **Aerospace Engineering** _____

Prof. Dr. Sinan Eyi
Supervisor, **Aerospace Engineering, METU** _____

Examining Committee Members:

Prof. Dr. Yusuf Özyörük
Aerospace Engineering, METU _____

Prof. Dr. Sinan Eyi
Aerospace Engineering, METU _____

Assoc. Prof. Dr. Nilay Sezer Uzol
Aerospace Engineering, METU _____

Assist. Prof. Dr. Mustafa Perçin
Aerospace Engineering, METU _____

Assist. Prof. Dr. Sıtkı Uslu
Mechanical Engineering, TOBB ETÜ _____

Date: 20.01.2023

I hereby declare that all information in this document has been obtained and presented in accordance with academic rules and ethical conduct. I also declare that, as required by these rules and conduct, I have fully cited and referenced all material and results that are not original to this work.

Name Last name : Rüştü Görkem Yılmaz

Signature :

ABSTRACT

EXTINGUISHMENT OF A SOLID ROCKET MOTOR BY RAPID DEPRESSURIZATION AFTER NOZZLE DETACHMENT

Yılmaz, Rüştü Görkem
Master of Science, Aerospace Engineering
Supervisor : Prof. Dr. Sinan Eyi

January 2023, 76 pages

In order to estimate the performance of a solid rocket motor with the nozzle detachment ability and to estimate the propellant extinguishment by rapid depressurization after detachment, a zero dimensional internal ballistic solver is developed, utilizing a transient burn rate model, which is to calculate the actual propellant burn rate at the rapid depressurization phase by solving the 1-D heat transfer equation within the propellant. As the detachable nozzle moves axially away from the motor by means of the ejecting force created by the chamber pressure, the solver also calculates the position of the detachable nozzle at every time instant, incrementing the effective gas discharge area of the motor, which is the cause of the rapid depressurization. For validation, static firings have been performed in which propellant extinguishment has been observed as estimated by the solver while the pressure transients calculated by the solver agreed well with the test results.

Keywords: Solid Rocket Motor, Transient Burning Rate, Extinguishment, Thrust Termination, Nozzle Detachment

ÖZ

KATI YAKITLI ROKET MOTORUNDA LÜLE AYRILMASI SONUCU ANİ BASINÇ DÜŞÜŞÜ İLE İTKİ SONLANDIRILMASI

Yılmaz, Rüştü Görkem
Yüksek Lisans, Havacılık ve Uzay Mühendisliği
Tez Yöneticisi: Prof. Dr. Sinan Eyi

Ocak 2023, 76 sayfa

Lüle fırlatma özelliğine sahip bir katı yakıtlı roket motorunun performansını ve lüle ayrılmasıyla oluşan ani basınç düşüşü sonucundaki yakıt sönmesini tahmin etmek amacıyla, zamana bağlı yanma hızı modeli kullanan sıfır boyutlu bir iç balistik çözücü geliştirilmiştir. Çözücü, katı yakıt içerisindeki 1 boyutlu ısı transferi denklemini çözerek, hızlı basınç düşüşü fazında anlık gerçekleşen yanma hızını hesaplamaktadır. Buna ek olarak, yanma odası basıncı sonucu oluşan kuvvet ile atılabilir lüle motordan ayrılırken, lülenin pozisyonunu her bir zaman adımında hesaplayarak basınç düşüşünün sebebi olan gaz tahliye açıklığı alanını her bir zaman adımında arttırmaktadır. Modelin doğrulanması için test motorları ile bir dizi statik ateşleme gerçekleştirilmiştir. Ateşlemelerde yakıtın söneceği çözücü tarafından tahmin edilmiş olup testlerde de yakıtın sönüp itkinin sonlandığı gözlemlenmiştir. Çözücü tarafından hesaplanan basınç zaman eğrileri ise ateşlemelerden elde edilen sonuçlarla örtüşmektedir.

Anahtar Kelimeler: Katı Yakıtlı Roket Motoru, Kararsız Yanma Hızı, Yanma Sonlanması, İtki Sonlandırma, Lüle Ayrılması

To my father…

ACKNOWLEDGMENTS

The author wishes to express his deepest gratitude to his supervisor Prof. Dr. Sinan Eyi for his invaluable support, advice and criticism throughout the research.

The author would also like to thank his colleagues Berkan Mumcu, Okan Ok, Merve Gözlükaya, Volkan Baydar, Mehmet Safa Aysan, Utku Olgun, Doğa Beşer, Berk Yurt, Tuğrul Akpolat, Kuzey Işıl, Berkan Zıraman, Özge Şen, Kağan Akın, Mesut Osman Akdoğan and Merve Bozdemir for their insight, heartfelt support and hard work, without which the validation tests could not be performed.

Special thanks to Ali Yıldırım for his insights, and for conducting the CFD analysis, which played a crucial role in the validation of the study and made it possible to view the problem in a much wider perspective.

The assistance and guidance of Osman Yücel and Korhan Coşkun in the development of the theory are gratefully acknowledged.

The author would like to express his additional appreciations to Roketsan for the infrastructure, hardware and encouragement for this work.

Finally, the author would like to thank his friends Duygu Tüfekçi Enginar, Onur Enginar, Alkan Kahraman, Hande Mert, Azer Mert, Gülçin Akarsu Şengöz and Oğuz Kerem Şengöz for their never-ending support, care and good company.

TABLE OF CONTENTS

LIST OF TABLES

TABLES

LIST OF FIGURES

FIGURES

LIST OF SYMBOLS

SYMBOLS

A_b	propellant burning surface area
A_{cs}	cross sectional area of the flow path at a point
A_e	cross sectional area of the nozzle exit section
A_t	cross sectional area of the nozzle throat section
a_P	empirical constant in the St. Robert's Law
α	thermal diffusivity of the propellant grain
C_P	heat capacity of the propellant
ΔH_i	net heat released or absorbed per unit mass of an ingredient of the propellant while dissociating
$d\vec{S}_{in}$	normal vector of an infinitesimal internal surface element
$d\vec{S}_{out}$	normal vector of an infinitesimal outer surface element
Δt	time increment
F	ratio of the heat required to gasify the propellant to the heat required to raise the temperature of the propellant to the surface temperature
γ	adiabatic index of the gas inside the motor
k_P	thermal conductivity of the propellant
λ	propellant heat of gasification
M	Mach number

M_t	Mach number at the nozzle throat section
m	mass inside the combustion chamber
m_i	mass fraction of a component in the propellant formulation
$\dot{m}$	mass flow rate
$\dot{m}_{in}$	mass flow rate entering the combustion chamber
$\dot{m}_{nozzle}$	mass flow rate leaving the combustion chamber
n_P	pressure exponent in the St. Robert's Law
p	pressure
p_{amb}	ambient pressure
p_c	chamber pressure
p_e	pressure at the nozzle exit section
p_t	pressure at the nozzle throat section
p_{total}	stagnation pressure at the nozzle entrance (chamber)
q_1	heat flux to the propellant solid from the surface
q_2	heat flux required to gasify the propellant with a given rate
q_3	heat flux from the gas phase to the propellant surface
r	steady state burn rate
R	non dimensional steady state burn rate
r_b	propellant burn rate
$r_{b,steady}$	steady state burn rate
$r_{b,unsteady}$	instantaneous burn rate at the rapid depressurization phase
R_{gas}	gas constant

$r_{unsteady}$	instantaneous burn rate at the rapid depressurization phase
$R_{unsteady}$	non dimensional instantaneous burn rate
r_0	steady-state burn rate at the instant of termination initiation
ρ	density of the gas inside the combustion chamber
ρ_P	density of the solid propellant
ρ_t	gas density at the throat section
t	time
T	temperature
T_c	combustion chamber (stagnation) temperature
T_s	surface temperature of the propellant
T_t	temperature at the nozzle throat section
T_{total}	stagnation temperature at the nozzle entrance (chamber)
T_0	initial conditioning temperature of the propellant
τ	non dimensional time
θ	non dimensional temperature
u_t	flow velocity at the nozzle throat section
V	combustion chamber free volume
v_e	flow velocity at the nozzle exit section
x	spatial coordinate inside the propellant grain
x^n	position of the detachable nozzle at the current time step
$\dot{x}^n$	velocity of the detachable nozzle at the current time step
$\ddot{x}^n$	acceleration of the detachable nozzle at the current time step

x^{n+1}	position of the detachable nozzle at the next time step
$\dot{x}^{n+1}$	velocity of the detachable nozzle at the next time step
Y	unitless coordinate inside the grain

CHAPTER 1

INTRODUCTION

Unlike a liquid propellant rocket engine, a solid rocket motor with a conventional design cannot be turned off during the burn time, which is a drawback when compared to a liquid engine. However, a solid rocket motor has its own advantages like simpler design, fewer number of components, better storability etc. So when there is a need for a propulsion system which is expected to bring a different level of total impulse at each mission for a system, which is achieved normally by a liquid engine, a solid rocket motor can offer a convenient solution if the extinguishment ability can be implemented.

In order to investigate the usability of a solid rocket motor as a propulsion system which can bring a level of total impulse differing from mission to mission, a solid rocket motor with a detachable nozzle was designed and manufactured in order to obtain propellant extinguishment by rapid depressurization when the nozzle is detached. In addition, a ballistic solver accompanied by an unsteady burn rate model was developed to predict the extinguishment phenomenon and to calculate the pressure and thrust transients of a solid rocket motor during the rapid depressurization phase. To validate the solver, multiple static firings with the aforementioned test motor were performed and the pressure-thrust curves obtained by the solver were compared to the ones produced by the test motors.

For the purpose of designing a solid rocket motor with the thrust termination capability, one needs a method to estimate the operational performance as well as the thrust termination compliance of the motor in the design phase, making sure that the motor would perform as intended before any static firing tests. The objectives of this thesis work is to investigate the physics of the combustion environment inside

the motor when extinguishment is taking place, to model the heat transfer inside the combustion chamber and the flow around the detachable nozzle with a simplistic approach, and finally come up with a complete performance estimation tool that is validated by static firing tests.

1.1 Literature Review

Literature review was conducted in the fields of dynamic burn rate estimation for solid propellants, prediction of solid rocket motor performance during thrust termination and solid propellant extinguishment estimation methods. A transient burning rate model which is able to capture the necessary physics of the combustion environment while being simplistic enough in order to be applicable to real life design scenarios was sought to have a transient burning rate model that would provide a basis for the modeling in this study. There are just a few studies conducted about the estimation of the propellant extinguishment in the literature. The ones which have been encountered are from the 70's. More recent studies that can be regarded as being relevant to the scope of this work are the ones about dynamic burn rate estimations for combustion instability simulations, which resemble the environment in an extinguishing rocket motor. In both subjects, actual burning rate is sought in an environment where the pressure is changing rapidly and similar assumptions are made about combustion.

Horton et al. (1968) conducted a study in which they offered a simplistic model which describes the heat transfer to the propellant surface and the combustion process of the propellant grain. They devised a set of equations which require a small handful of propellant thermophysical properties. Being rather simplistic, these equations include some assumptions which need to be justified through empirical results. Probably the most important assumption of the model is that the rate of the heat transfer from the combustion gases to the propellant surface being pressure dependent only. This means that the gas phase can be assumed to reach its steady condition very rapidly compared to the solid phase (propellant grain). Namely, in the

combustion environment where the chamber pressure changes rapidly, for some pressure value at a time instant, the combustion gases transfer the heat energy with the same rate as they would in an environment where the pressure is constant. In the paper, this assumption is justified by comparing the characteristic times of the gas phase and the solid phase, stating that the characteristic time of the solid phase is about an order of magnitude greater than that of the gas phase. In order to validate the proposed method, the authors performed a series of static firings in which they opened an auxiliary nozzle while the motors were operating steadily, and compared the results of the extinguishing and non-extinguishing cases with the results of the method. In the most of the cases, the method predicted the extinguishment and non-extinguishment correctly. The shortcoming of the study is that the authors did not couple the model with an internal ballistic calculator which could produce pressure vs. time data to feed the necessary inputs to the model in order to proceed with the solution. Instead, they used the pressure vs. time output of a particular test to estimate the results of the firings. So, while being extremely valuable for explaining the physics of the heat transfer taking place in the combustion chamber and introducing very practical simplifications to the process, this work does not constitute a complete solution to the extinguishment problem unless it is coupled with an internal ballistic solver.

Kumar (2007) proposed a dynamic burn rate model which involves a propellant parameter called “extinction compliance”, and maintains that it is an effective and simplistic model unlike some other models proposed in the past, which are evaluated by the author as too complicated for practical applications. The mathematical model relates the actual burn rate of the propellant to the extinction compliance, which is formulated as the ratio of the instantaneous pressure and the steady-state burn rate. In the offered methodology, the extinction compliance of the propellant, which is a function of time, is extracted by determining the function constants that yield the dynamic burn rate relation which fits best to the time history of the unsteady burn rate recorded in the depressurization tests of the propellant in question. The author states that for a propellant, depressurization tests provide unique and repeatable

results with less ambiguity and data scatter. The resultant equation for the instantaneous burn rate is a relation which involves the time derivative of pressure and the extinction compliance. In the model, the assumed form of the extinction compliance is an exponential function with some constants to be determined experimentally. The simple form of the extinction compliance function makes the simplistic form of the burn rate equation possible. In order to validate the model, the author used the results of two depressurization tests which have been performed by Suhas and Bose (1980). In order to calculate the time history of the transient burn rate that was recorded in the experiments, the author used the pressure vs. time data from the experiments and determined the constants of the extinction compliance function by fetching the constants which produce the best fit to the experimental burn rate history when substituted into the burn rate equation. For the both experiments, the calculated burn rate vs. time data capture the experimental burn rate history quite well at the majority of the data points. While producing encouraging results and being simplistic in form, this model requires a depressurization test to be performed on the propellant and the functional constants to be obtained before it can be used in a real rocket motor performance simulation. Hence it is not a completely thorough model which does not require any empirical properties.

For the purpose of estimating the transient combustion response of a solid rocket motor to unsteady flow field behavior, also known as combustion instability, Greatrix (2008) suggested a general transient burning rate model which calculates the instantaneous burn rate of a propellant. In order to estimate the instantaneous burning rate, the model employs the entire temperature distribution inside the solid propellant grain unlike the past models, which utilize the thermal gradient at the propellant surface. Offered model is described as a general burn rate model, meaning that it can be employed for any burn rate mechanism such as pressure, core mass flux, etc. Similar to the methodology suggested by Horton et al. (1968), the temperature distribution along the propellant solid is solved at every time step. Furthermore, the model offered by Greatrix (2008) utilizes the steady-state burning rate when calculating the heat conducted by the gas phase to the propellant surface,

which is needed for a closed set of equations solving for the heat conduction inside the solid phase. Meaning that the heat input of the gas phase at a time insant is calculated by using the amount of propellant that it would burn in an environment where the flow parameters do not change rapidly with time but the parameters are equal to that particular time instant. This practice requires the assumption of a gas phase behaving as it is steady (a gas phase which converges rapidly to the steady phase), which is the same assumption used by Horton et al. (1968). In the study, a variable propellant surface temperature is tried by using an Arrhenius type function which relates the surface temperature to the actual burning rate. It is reported that a constant surface temperature conformed to the experimental results better, so a constant propellant surface temperature assumption is used when producing the results. It is also reported that the model was unstable originally and there was a need for an equation which physically constrains the diverging burn rate. For this purpose, an empirical correlation for the time derivative of the burn rate, which bounds the value of the burn rate, is used. Since this equation is empirical, the empirical constants of the equation have to be determined for the propellant in question (most probably by T-burner experiments). This need for an empirical correlation factor necessitates some additional tests to be performed on the propellant and can be seen as a drawback when evaluating the applicability of the method.

1.2 Working Principle of a Solid Rocket Motor

A solid rocket motor can be considered as a pressure vessel with a built-in gas generator which pressurizes the system. Normally, this built-in gas generator is a solid propellant grain which contains its own fuel-oxidizer mixture and the rocket motor continues to operate and produce thrust until the solid propellant grain is depleted. Essentially, the rate of the mass flow entering the motor from the propellant surface and the rate of the mass flow leaving the motor from the predefined nozzle throat area determine the chamber pressure, which in turn generate the thrust force. The forces acting on a typical solid rocket motor are illustrated in Figure 1.1. The

force balance on the total surface area of the motor is the generated thrust. The forces acting on the inner surface of the motor are caused by the pressure generated by the propellant burn in the combustion chamber and the gas flow through the nozzle. The forces acting on the outer surface of the motor are caused by the ambient atmosphere and in the case of a static firing, this is the static pressure of the atmosphere since the motor is held stationary.

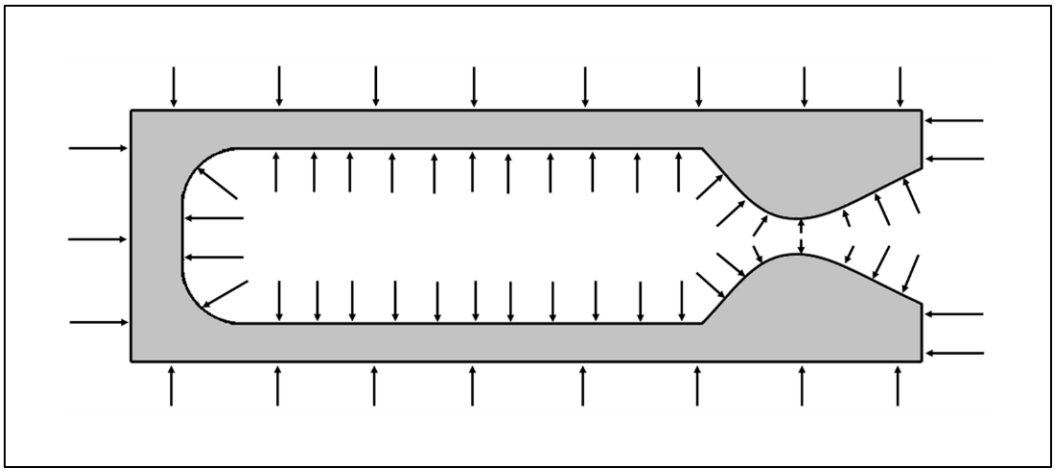

Figure 1.1. Forces acting on a solid rocket motor

The surface integral of the pressure inside the motor can be found by the conservation of momentum.

$$\oint \vec{p} \cdot d\vec{S}_{in} = \dot{m} v_e + p_e A_e \qquad (1.1)$$

where $\dot{m}$ is the mass flow rate leaving the rocket motor, v_e, p_e and A_e are the flow velocity, static pressure and cross sectional area at the nozzle exit respectively.

For the outer surface of a solid rocket motor undergoing a static firing, the net force can be calculated by the surface integral of the pressure as well. Since the same static pressure is applied to every outer surface, the forces acting on the opposite surfaces cancel out. Namely,

$$\oint \vec{p} \cdot d\vec{S}_{out} = -p_{amb} A_e \qquad (1.2)$$

where p_{amb} is the ambient pressure. Since the net force acting on the motor is the sum of the surface integrals of pressure acting on the inner and outer surfaces, the net force hence the thrust output of a solid rocket motor can be calculated as such:

$$\oint \vec{p} \cdot d\vec{S}_{in} + \oint \vec{p} \cdot d\vec{S}_{out} = Thrust = \dot{m} v_e + (p_e - p_{amb}) A_e \qquad (1.3)$$

In order to obtain a pressure distribution throughout the motor which is to produce thrust, high pressures are needed inside the combustion chamber. For a solid rocket motor, the source of the chamber pressure is the gaseous combustion products of the burning solid propellant grain.

Prior to rocket operation, the propellant grain remains unburned and an igniter is needed to initiate the burn. The igniter of a solid rocket motor is typically a pyrotechnic device which contains compacted gunpowder like chemicals that rapidly eject jets of high temperature gases to the surfaces of the solid propellant grain upon activation. The igniter gets initiated typically by a heated electric wire, which is heated by a specific electric current for a specific amount of time. When the igniter is activated, it transfers the necessary initial heat to the propellant via the high temperature jets.

As a result of the heat transfer by igniter operation, the contents of the propellant start to gasify through pyrolysis and dissociative sublimation (Keenan & Siegmund, 1969). At this point, this unburned gas mixture undergoes combustion reactions, which produce high levels of heat, which is in turn transferred to the propellant surface in order to provide the necessary energy for the gasification of the solid propellant. The combustion reactions feed in the heat energy for the mass ejection to occur and the mass ejection from the surface provides the reactants for the combustion reactions as a self contained loop. So once the burn is initiated, the propellant can sustain its own burn.

The main ingredients of a typical solid propellant grain are the oxidizer and the fuel, which are in a solid form before the dissociation reactions at the surface. The oxidizer is a chemical compound, which releases oxygen when it gets decomposed at the

surface. The fuel, which is typically a hydrocarbon, undergoes pyrolysis at the propellant surface and reacts with the oxygen which is provided by the oxidizer (Cohen, Fleming & Derr, 1974). This combustion reaction takes place at a distance from the propellant surface and is the source of the energy for the rocket operation. In some applications, a particular amount of powder aluminum is added to the propellant formulation for the purpose of increasing the energy inside the combustion chamber, since aluminum releases a high amount of energy when reacting with oxygen, which increases the chamber pressure and the temperature inside the combustion chamber.

In a short while after ignition, the high pressure combustion products, which can be assumed to be stagnant in the combustion chamber, start to get accelerated at the nozzle entrance and reach to the sonic velocity at the nozzle throat, which is called the chocked condition. Downstream of the throat of a supersonic nozzle, the flow area is continously expanded by increasing the nozzle cross sectional area. The flow is further accelerated to the supersonic speeds by this expansion, which in turn increases the momentum. The area ratio between the nozzle exit area and the throat area is called the expansion ratio and it is a design parameter which is mainly driven by the ambient pressure at the operation altitude of the rocket. As the operation altitude increases, the expansion ratio, which is designated in the design, is set to be a higher value compared to a rocket motor operating in a lower altitude.

The time rate of chamber pressure change in a solid rocket motor is a strong function of the burn rate of the propellant, which is in turn a function of the chamber pressure. The propellant burn rate can be thought as the regression rate of the solid propellant surface. When estimating the performance (calculating the pressure and thrust vs. time curves) of a typical solid rocket motor, function of the burn rate with respect to pressure, which is a propellant property, is fed to the internal ballistic solvers as an input. This propellant property can be measured by different techiques which involve a small scale propellant sample with the same formulation of the propellant whose burn rate is sought. The most common burn rate measurement procedures are the usage of strand burners, ultrasonic burn rate measurement devices and small scale

test motors, in which a predefined amount of propellant with a known web thickness is cast into a test motor and the burn rate data are extracted by simply dividing the web of the propellant grain by the burn time. Design of the test motor geometry ensures a near constant chamber pressure to obtain a single burn rate value corresponding to a single pressure level. Multiple test motors with different operating pressures (motors having different nozzle throat areas) have to be fired in order to obtain the burn rate as a function of pressure.

1.3 Motivation Behind the Utilization of a Solid Rocket Motor Instead of a Liquid Engine in a Thrust Terminating System

Typically, a liquid propellant rocket engine is employed when there is a need for an on/off switch. Since the oxidizer and the fuel are stored in separate tanks and are fed to the thrust chamber by pumps and valves, the supply can be cut and restarted in order to kill and restart the engine. Furthermore, the engine can be throttled since the flow rate of the fuel and oxidizer can be adjusted by the pumps and valves.

Unlike a liquid engine, a conventional solid propellant rocket motor cannot be turned off during the burn, since the propellant combustion is self-sustained in the combustion chamber. So once the burn is initiated, the combustion continues until the grain burns out, which means that a typical solid rocket motor outputs the same total impulse (time integral of the thrust output) in every flight. So, a solid rocket motor is employed generally when the system does not require the extra features of a liquid engine (as the boosters of space systems or on missiles). On the other hand, a liquid engine is the choice for the systems which require thrust control (mostly space applications).

As mentioned above, a liquid engine provides some abilities like throttling, on/off capability, etc. However, liquid engines have some drawbacks like the challenges in their design and operation, caused by the complicated system architecture which involves intricate cycles and rotary parts like the turbopumps. Additionally, liquid

fuel introduces additional challenges which need to be overcome in terms of storability, caused by the abrasive characteristic of some liquid fuels, which means that compared to a liquid fuel, it is more convenient to store a solid propellant, since a typical solid propellant grain is bonded to the liner in the motor case, with hardly any chemical interaction with the surroundings. Furthermore, generally a solid motor can be packed more compactly to a system since there are no additional fuel and oxidizer tanks like a liquid engine, which would need additional space. A solid rocket motor also provides a simplistic architecture which does not involve any rotary part or any fuel/oxidizer line, absence of which reduces the cost of the design significantly.

The essence of what is stated above is that, if there is a need for a propulsion system with the capability of thrust termination and no additional liquid engine features like restarting or throttling are needed, a solid rocket motor with the thrust termination capability would prove to be a convenient alternative to a liquid engine, especially when its advantages listed above are considered. So when a vehicle requires a propulsion system which is to bring a different level of total impulse at each mission, a solid rocket motor which has a thrust termination mechanism can be considered as a feasible option thanks to its simplicity and better storability.

1.4 Outline of the Thesis Report

In Chapter 2, the methodology that is used for thrust termination and the modeling efforts for the purpose of estimating the performance for both normal operation and termination are discussed. First, the reasons behind the selection of nozzle detachment technique for terminating the thrust are given. Then, the working principle of the thrust terminating test motor is described. Afterwards, the method and the steps of the motor operation and termination simulation are elaborated. In this part, the solver processes are explained and the governing equations are presented with solution methods.

In Chapter 3, the properties of the test motors that are developed for validation purposes are presented with the scenario of each test. After that, the results of the tests and the fidelity of the solver are discussed with some comparisons between test data and solver output.

In Chapter 4, some conclusions regarding the feasibility of a thrust terminating solid rocket motor are given, and some points to consider in the design phase of a thrust terminating system are mentioned. Finally, the overall performance and the sufficiency of the solver when it is used in such a problem are evaluated.

CHAPTER 2

THRUST TERMINATION TECHNIQUE AND ITS PHYSICAL SIMULATION

In this study, thrust termination by solid propellant extinguishment is achieved by decreasing the chamber pressure rapidly. For the purpose of estimating the performance of a thrust terminating solid rocket motor in its normal operation phase or in its thrust termination phase where the chamber pressure drops drastically by the effect of nozzle detachment, the propellant burn rate has to be known at every time instant during the simulation.

For a given motor design, in order to calculate the actual propellant burn rate and pressure at each time step during rapid depressurization, one needs a dynamic burn rate model, since the actual burn rate of the propellant during a rapid pressure change differs significantly from its steady state burn rate, which is calculated by the typical relations like St. Robert's Law (the curve fitted to the burn rate vs. pressure data extracted from the small scale burn rate measurements). Namely, these methods which yield the steady-state burn rate are sufficient for the burn rate estimation of a motor in its steady operation phase, but while the chamber pressure is changing steeply, a method is required to calculate the actual burn rate. For this reason, a method requiring a few propellant thermochemical properties is employed when calculating the unsteady burn rate.

For a given time instant in the transient phase, 1-D heat conduction equation for the propellant solid, and the equation for the heat conducted from the propellant surface to the solid are solved simultaneously. The implicit numerical solution of these two equations with the appropriate initial and boundary conditions result in the 1-D temperature distribution inside the propellant and the unsteady burn rate at a given time instant.

2.1 Working Principle of the Thrust Terminating Solid Rocket Motor Devised for the Study

A solid rocket motor is designed and manufactured for the purpose of investigating the feasibility of the thrust termination concept and to test the capability of the solver which is developed for this study in estimating the solid propellant extinguishment (when the burn rate equals zero) as well as the pressure and thrust histories produced by a solid rocket motor while the chamber pressure is falling drastically.

In this study, nozzle detachment is the method which is used in order to drop the chamber pressure steeply and reach to the point of extinguishment, hence thrust termination. There are some other existing methods which are used for the purpose of thrust termination like spraying water to the burning propellant surface (Taback, Day & Browne, 1965), which helps to reduce the propellant surface and chamber temperature, or suddenly opening venting holes in the combustion chamber in order to drop the chamber pressure, or opening auxiliary nozzles at the head end of the motor, which creates additional reverse thrust to neutralize the thrust output.

Depressurization by nozzle detachment is selected for this study because of its simplicity in design and manufacture. Since the nozzle is readily being pushed away by the chamber pressure and the only element that is holding the nozzle from being ejected from the motor is the detachment mechanism, the nozzle can be easily detached without an additional energy source when the detachment mechanism is invoked.

Extinguishment by water spray would require an intricate spray and hose system for the water purge with an additional tank to pressurize the water discharge system, whose complications would invalidate the simplisity benefit of a solid rocket motor.

The concept of suddenly opening some venting holes in the combustion chamber is similar to the concept of nozzle detachment, both suddenly depressurizing the combustion chamber to achieve extinguishment. In a sense, both methods can be considered to be the same, since the same governing equations apply. The venting

hole concept is not used for this study because of the extra challenges that would be brought by the drilling and sealing of the motor case, which is also the reason behind the dismissal of the concept in which auxiliary nozzles create reverse thrust at the head end of the motor.

So, nozzle detachment is selected as the method to be used for the purpose of suddenly decreasing the chamber pressure in order to achieve propellant extinguishment and thrust termination.

Figure 2.1 illustrates the thrust terminating solid rocket motor which is devised for the study and Figure 2.2 illustrates how the effective gas discharge area of the motor gradually increases as the detachable nozzle moves axially away from the motor, decreasing the chamber pressure. The architecture of the thrust terminating solid propellant rocket motor which is designed for this study employes two nozzles, one of which is located radially outward and being held in its place by bonding agents and bolted connections, meaning that it is stationary. The other nozzle, which is located inside the hole of the outer nozzle, is a solid component that is not bonded to the remaining subcomponents of the motor and is free to move in the thrust axis. This component is called the detachable nozzle and it is locked in its position by a mechanism, whose details and working principle is outside of the scope of this study. During the operation of the rocket motor, this mechanism holds the detachable nozzle in its place and counteracts the ejecting forces applied by the chamber pressure.

At a time instant where the nozzle detachment mechanism gets activated, the detachable nozzle becomes free and it starts its axial motion away from the motor. An annular discharge area appears shortly after the detachable nozzle starts to move away from the motor. As the time progresses, the nozzle is ejected further away by means of the chamber pressure, and this secondary annular discharge area grows at every time step until the detachable nozzle leaves the motor entirely. When the detachable nozzle is completely ejected, the effective gas discharge area of the motor becomes the throat area of the outer nozzle. This rapid growth of the discharge area

acts as a factor which decreases the chamber pressure dramatically and the rapid pressure drop causes the solid propellant to be extinguished at some point, thus terminating the thrust.

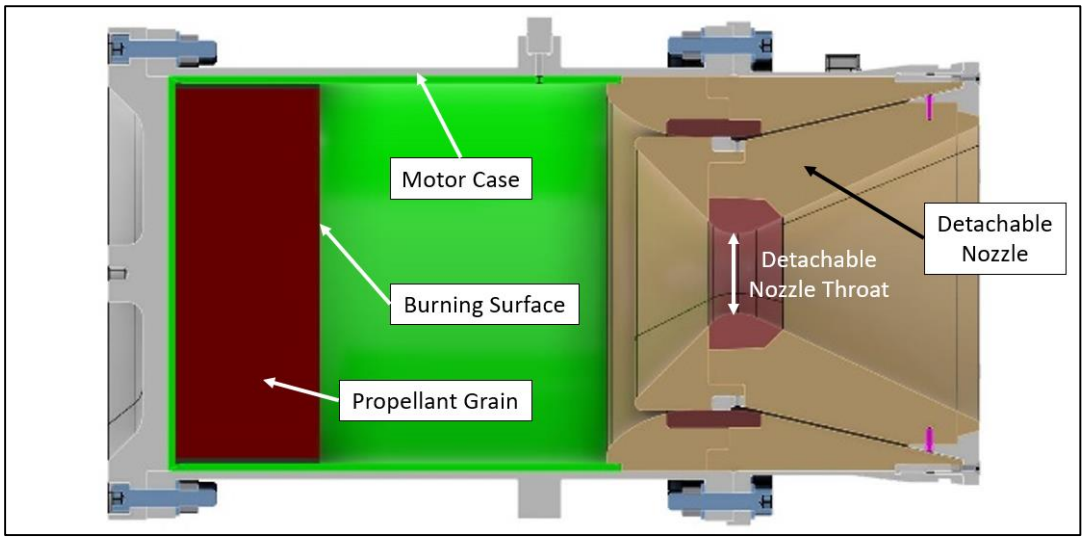

Figure 2.1. Side view of the thrust terminating solid rocket motor

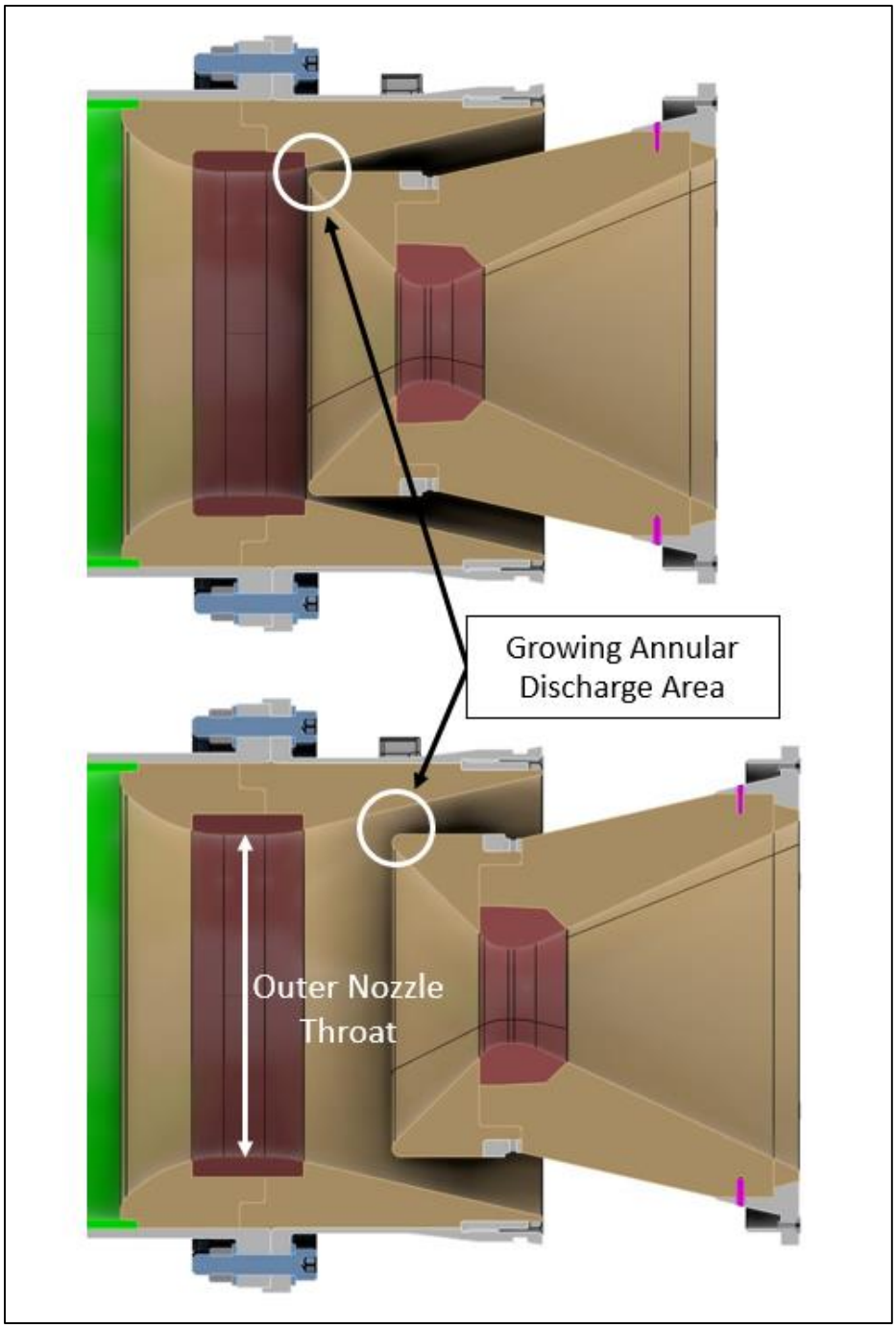

Figure 2.2. Growth of the annular area

2.2 Simulation of the Rocket Operation and Termination

2.2.1 General Structure of the Simulation

A zero dimensional internal ballistic solver is developed for the purpose of estimating the performance parameters like pressure and thrust of a solid propellant rocket motor during normal operation and thrust termination phases. The basis of the solver can be regarded as an ordinary 0-D internal ballistics calculator. The solution algorithm of the 0-D solver is expanded by the addition of a transient burning rate model which calculates the actual burning rate while the pressure drops steeply and a simulation for the detachable nozzle motion which calculates the position of the nozzle in motion and the effective discharge area in each time step to feed in the necessary input for the transient calculations.

The aforementioned solver is a simulation tool which essentially calculates the inner pressure vs. time of a pressure vessel, which is pressurized by the gas generated by the burning propellant. At each time step, the chamber pressure increment is calculated by a mass balance equation which relates the time derivative of the chamber pressure to the difference between the mass flow rates entering and leaving the motor.

In order to calculate the mass flow rate entering the combustion chamber, the solver uses propellant burn rate, which is a function of pressure. Isentropic relations are used to calculate the mass flow rate leaving the motor from the nozzle throat. Other parameters like thrust etc. can be derived by the isentropic relations as well.

After initializing the pressure and the corresponding burn rate, at each time step the pressure is updated, taking the changing propellant burn area, increasing chamber volume and nozzle throat erosion into account. Additionally, the developed solver takes the annular discharge area, which is calculated using the detachable nozzle position, at each time step and adds it to the nozzle throat area when calculating the

mass discharge from the motor. Also, a module for the transient burning rate calculations is invoked at this phase to calculate the mass generation rate.

Prior to nozzle detachment, the internal ballistic solver uses the steady state burn rate to calculate pressure vs time. When the nozzle detachment is initiated, the internal ballistic solver switches to the transient burning rate model to calculate the unsteady burn rate and uses that information to find the pressure at the new time instant. The performance parameters are calculated while marching in time and as the effective discharge area of the flow leaving the combustion chamber gradually increases because of the detachment, the pressure and the actual burn rate decreases steeply over time and the propellant is said to be extinguished when $r_{b,unsteady} = 0$.

Figure 2.2 illustrates the geometry of the domain in which an annular discharge area appears when the detachable nozzle starts to move away from the motor. As the time progresses, the nozzle is ejected further away by means of the chamber pressure, and this secondary annular discharge area grows at every time step until the detachable nozzle leaves the motor entirely. This rapid growth of the discharge area acts as a factor which decreases the chamber pressure dramatically and the rapid pressure drop causes the solid propellant to be extinguished at some point, thus terminating the thrust. Figure 2.3 illustrates the general structure of the internal ballistics solver.

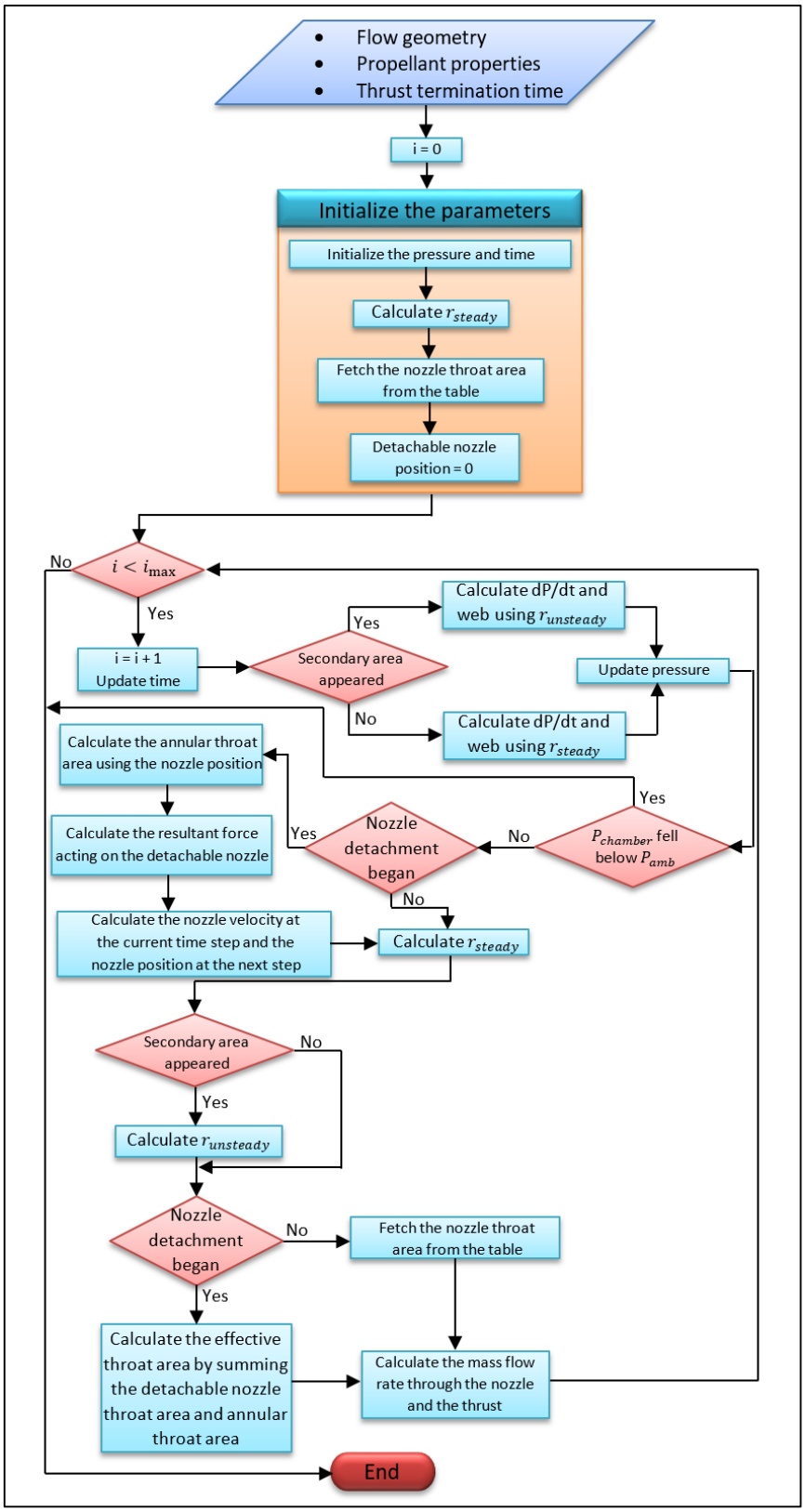

Figure 2.3. Flowchart of the ballistic solver

Solver takes the inputs such as the flow geometry parameters like shapes of the detachable nozzle and the outer nozzle, instances of which are given in Figure 2.2. Alongside some other inputs, solver also takes the propellant properties like the steady-state burn rate vs. pressure, burn area vs. web burned, etc.

Upon initiation, solver fills in the initial values of chamber pressure, internal volume, mass flow rate into and out of the combustion chamber, etc. Detachable nozzle position starts from zero and the calculations are made in a fashion similar to an ordinary 0-D solver until the thrust termination time, which is a solver input, is reached. In this phase which is between initiation and termination, for each time step the time derivative of chamber pressure, which is mainly a function of propellant burn rate, throat area, chamber volume and temperature, is calculated. After that, the derivative is multiplied by the time step size in order to update the chamber pressure for the current time step. Then, the propellant burn rate is calculated using the chamber pressure. At this stage, the steady-state burn rate equation which is given by (2.1) is used.

$$r_{b,steady} = a_P p^{n_P} \qquad (2.1)$$

Here, p is the chamber pressure of the current time step, n_P is the pressure exponent of the propellant and a_P is a constant. This equation, which relates the burn rate to the pressure and some propellant properties, is known as St. Robert's Law and it can describe the propellant burn rate for a wide range of pressure values. The constants a_P and n_P can be found by a series of small scale test motor firings for different chamber pressure values. At each test firing, a burn rate value is obtained for a particular chamber pressure. After say three different tests for three different pressures, a graph with three data points, each point representing a burn rate value at a particular pressure, is obtained. Fitting a power law to the point set, one can find the constants a_P and n_P for the propellant in question which in turn results in a burn rate relation for pressure values varying in a range.

At a time instant, propellant burn rate is used in order to calculate the mass flow rate into the combustion chamber. In turn, this mass flow rate is used in the calculation

of the time derivative of pressure, whose product with the time increment gives the chamber pressure at the next time step. St. Robert's Law can be used for the burn rate calculations while there are mild changes in the chamber pressure (during the operation of a typical solid rocket motor except the ignition transient phase). As a result, this law is used for the mass flow rate into the combustion chamber while the motor is in its normal operation phase and the transient burn rate model, whose details are discussed in the subsequent chapters, is used after the termination in the solver.

After the calculation of burn rate, nozzle throat area is found by interpolation from a table which is a user input, giving the throat area values at different time instants. The reason behind this area change is the erosion of the material that is used for the nozzle throat insert. Throat area is used for the purpose of calculating the rate of the mass flow out of the motor, which is a part of the pressure derivative equation together with the mass flow rate into the combustion chamber. Following the calculation of the mass flow rate through the nozzle, thrust is calculated using the isentropic relations. These calculations are made for every time step and the performance parameters such as the chamber pressure and the thrust are recorded while incrementing the time.

Starting from the point where the thrust termination is initiated (the point at which the detachable nozzle is released and free to move axially away from the motor), the solver proceeds with the solution in a manner quite similar to the earlier phase described above. Compared to the normal operation phase, the additional processes that take place in the thrust termination phase are the calculation of nozzle position and the corresponding auxiliary throat area (to be summed up with the detachable nozzle throat area in order to calculate the total mass discharge area), propellant burn rate calculation using the dynamic burn rate model, and the calculation of the internal volume and the change rate of internal volume by taking the influence of the moving nozzle on the combustion chamber geometry into account.

2.2.2 Chamber Pressure Calculation

2.2.2.1 Equation for the Time Derivative of Pressure

For the purpose of calculating the chamber pressure at each time step, an equation describing the change rate of pressure, which can be derived from the conservation of mass, is used. Conservation of mass in the combustion chamber of a solid rocket motor can be stated as such:

$$\frac{dm}{dt} = \dot{m}_{in} - \dot{m}_{nozzle} \qquad (2.2)$$

where m denotes the mass of the combustion products inside the combustion chamber, $\dot{m}_{in}$ the mass flow rate entering and $\dot{m}_{nozzle}$ the mass flow rate leaving the combustion chamber, and t is the time.

Rewriting m as $m = \rho V$ where ρ is the density of the combustion products inside the combustion chamber and V is the chamber free volume,

$$\frac{dm}{dt} = V\frac{d\rho}{dt} + \rho\frac{dV}{dt} = \dot{m}_{in} - \dot{m}_{nozzle} \qquad (2.3)$$

In (2.3), an assumption is made that the flow variables are independent of the axial location inside the combustion chamber, i.e. the parameters like density and pressure do not vary inside the combustion chamber at a time instant. This assumption becomes invalid for long motors, variation of the flow parameters becomes significant in whose combustion chambers.

Using the ideal gas law to write ρ in terms of the chamber pressure p,

$$\rho = \frac{p}{R_{gas}T} \qquad (2.4)$$

$$\frac{d\rho}{dt} = \frac{1}{R_{gas}T}\frac{dp}{dt} \qquad (2.5)$$

where R_{gas} is the gas constant. In (2.5), it is assumed that the temperature T of the combustion products inside the combustion chamber is a constant. This property is a function of propellant formulation and stagnation pressure and is commonly obtained through the thermochemical analysis tools like CEA, released by NASA. The combustion chamber (stagnation) temperature generally varies little with changing stagnation pressure, therefore it is assumed to be constant and is denoted by T_c from this point in the derivation. Substituting (2.4) and (2.5) into (2.3),

$$\frac{V}{R_{gas}T_c}\frac{dp}{dt} + \frac{p}{R_{gas}T_c}\frac{dV}{dt} = \dot{m}_{in} - \dot{m}_{nozzle} \qquad (2.6)$$

Orginizing the terms in (2.6),

$$\frac{dp}{dt} = \frac{1}{V}\left(R_{gas}T_c(\dot{m}_{in} - \dot{m}_{nozzle}) - p\frac{dV}{dt}\right) \qquad (2.7)$$

Observing (2.7) and considering the assumptions, it can be deduced that the time rate of pressure change inside the combustion chamber is dependent upon the rate of change and the instantaneous value of the chamber volume, instantaneous chamber pressure, temperature and the net rate of change of the mass inside the chamber.

2.2.2.2 Calculation of the Mass Flow Rate into the Combustion Chamber

$\dot{m}_{in}$, the rate of the propellant mass flow into the combustion chamber, can be written as,

$$\dot{m}_{in} = \rho_P r_b A_b \qquad (2.8)$$

where ρ_P is the solid propellant density, r_b is the propellant burn rate and A_b is the propellant burning surface area. Propellant density is assumed to be constant and the propellant burn rate r_b can be calculated by St. Robert's Law or the dynamic burn rate model, depending on the phase that the motor is in. Burning surface area A_b is a geometrical property and it is a function of the propellant's web thickness at a time instant during the burn. Since the pressure is assumed not to be varying inside the

chamber, at a time instant the burned thickness of the propellant is the same at every part of the propellant grain. Hence, the value of burning surface area vs. the burned web thickness becomes merely a geometric property. The shape of the initial burning surface of the grain is the main parameter that influences the burn area vs. web of a propellant, which can be calculated by specialized tools that deform the surface of the grain by small increments until the end of the propellant grain shape. The end product of these tools are generally the burn area vs. web data of the propellant. The solver that is developed for this study takes the burn area vs. web data as an input. So in the simulation, it keeps track of the burned web thickness at every time instant and calculates the burn area corresponding to the web thickness at a time instant by interpolating the input data.

In addition to $\dot{m}_{in}$, instantaneous burn area is used for calculating V and $\frac{dV}{dt}$ as well. Since the chamber free volume is influenced by the propellant volume, the change rate of propellant volume would be equal to the change rate of chamber volume and it can be calculated by multiplying the burn rate by the burn area. In the thrust termination phase, the effect of nozzle position on the chamber volume is added to the volume change caused by the propellant burn in order to obtain the total volume change.

2.2.2.3 Calculation of the Mass Flow Rate Through the Nozzle

$\dot{m}_{nozzle}$, the rate of the mass flow leaving the combustion chamber through the nozzle throat, can be derived using the isentropic relations. Mass flow rate through the cross sectional area of the nozzle throat can be written as,

$$\dot{m}_t = \rho_t A_t u_t \qquad (2.9)$$

where ρ_t is the gas density, A_t is the cross sectional area and u_t is the flow velocity at the throat section. Using the perfect gas relation which is given by (2.4), above equation can be written as,

$$\dot{m}_t = \frac{p_t}{R_{gas}T_t} A_t u_t \quad (2.10)$$

where p_t is the pressure and T_t is the temperature at the throat section. Assuming the flow is sonic at the throat,

$$u_t = \sqrt{\gamma R_{gas} T_t} \quad (2.11)$$

where γ is the ratio of the specific heats of the gasses inside the motor. T_t can be rewritten assuming isentropic conditions inside the rocket motor.

$$T_t = \frac{T_{total}}{1 + \frac{\gamma - 1}{2} M_t^2} \quad (2.12)$$

where T_{total} is the total (stagnation) temperature at the nozzle entrance and M_t is the Mach number at the throat. For the majority of the solid rocket motors, the gasses at the nozzle entrance can be assumed to be stagnant and the whole combustion chamber can be treated as one station that is in stagnation when performing ballistic performance estimations (except for the ones with high length to diameter ratios). In addition, the flow through the nozzle can be assumed to be isentropic. So, the region before the nozzle entrance is treated as one station with stagnation conditions in this study. Since the flow is sonic at the throat,

$$M_t = 1 \quad (2.13)$$

$$T_t = \frac{T_{total}}{1 + \frac{\gamma - 1}{2}} \quad (2.14)$$

$$T_t = \frac{2T_{total}}{\gamma + 1} \quad (2.15)$$

(2.11) can be restated using (2.15).

$$u_t = \sqrt{\frac{2\gamma}{\gamma + 1} R_{gas} T_{total}} \quad (2.16)$$

Again using isentropic flow assumption to rewrite p_t,

$$p_t = \frac{p_{total}}{\left(\frac{\gamma+1}{2}\right)^{\frac{\gamma}{\gamma-1}}} \quad (2.17)$$

where p_{total} is the stagnation pressure at the nozzle entrance (or chamber). Substituting (2.15), (2.16) and (2.17) into (2.10) and rearranging,

$$\dot{m}_t = \dot{m}_{nozzle} = p_{total} A_t \gamma \sqrt{\left(\frac{2}{\gamma+1}\right)^{\frac{\gamma+1}{\gamma-1}} \frac{1}{\gamma R_{gas} T_{total}}} \quad (2.18)$$

The subscript $total$, denoting the stagnation values at the nozzle entrance section, is replaced with the subscript c in order to emphasize that the flow conditions are assumed to be the same in the entire combustion chamber. Therefore,

$$\dot{m}_{nozzle} = p_c A_t \gamma \sqrt{\left(\frac{2}{\gamma+1}\right)^{\frac{\gamma+1}{\gamma-1}} \frac{1}{\gamma R_{gas} T_c}} \quad (2.19)$$

where p_c and T_c denote the chamber pressure and temperature respectively. As it was discussed previously, the chamber temperature T_c is assumed to be a constant and a propellant property.

Observing (2.7) and (2.19), one can notice that the mass flow rate through the nozzle increases with increasing chamber pressure. In turn, increasing mass flow rate leaving the chamber reduces the chamber pressure. Therefore, $\dot{m}_{nozzle}$ and p_c are the two parameters balancing each other during the operation of a solid rocket motor. This effect can be seen in the rapid pressurization phase taking place in the first few milliseconds in a static firing, in which the rapidly increasing pressure gets limited by the increasing $\dot{m}_{nozzle}$ in a short amount of time.

2.2.3 Simulation of the Detachable Nozzle Motion

In order to calculate the chamber pressure using (2.7) for every time step after the instant at which the detachable nozzle becomes free, the sum of the cross sectional areas of all openings that are created and through which the gasses are discharged has to be known. At the termination phase where the detachable nozzle moves axially, the gasses inside the motor are discharged through the throat section of the detachable nozzle as they normally do in the normal operation phase. Additionally, the gasses start to escape through the annular channel that is formed between the outer surface of the detachable nozzle and the inner surface of the outer nozzle after the detachable nozzle passes a certain location during its motion. The annular channel around the detachable nozzle that is formed during the motion of the nozzle is illustrated in Figure 2.2.

When calculating the total cross sectional area of the openings that the mass is discharged through, the throat area of the detachable nozzle and the throat area of the annular channel are summed together to obtain the effective throat area of the motor, which is used as the value of A_t in (2.19) to calculate the rate of the mass flow leaving the motor.

The cross sections that the gas flow passes through are calculated for the entire length of the annular channel at every time instant. Figure 2.4 illustrates the orientations and the annular thicknesses of the channel cross sections at several exemplary nozzle positions, which are calculated by the solver. The cross sections are calculated and thus visible for the positions in which the detachable nozzle has moved enough to form a gas passage between the detachable nozzle and the outer nozzle. As it can be observed from Figure 2.4, as soon as a passage is formed, the cross sections are calculated at the locations on the surface of the detachable nozzle.

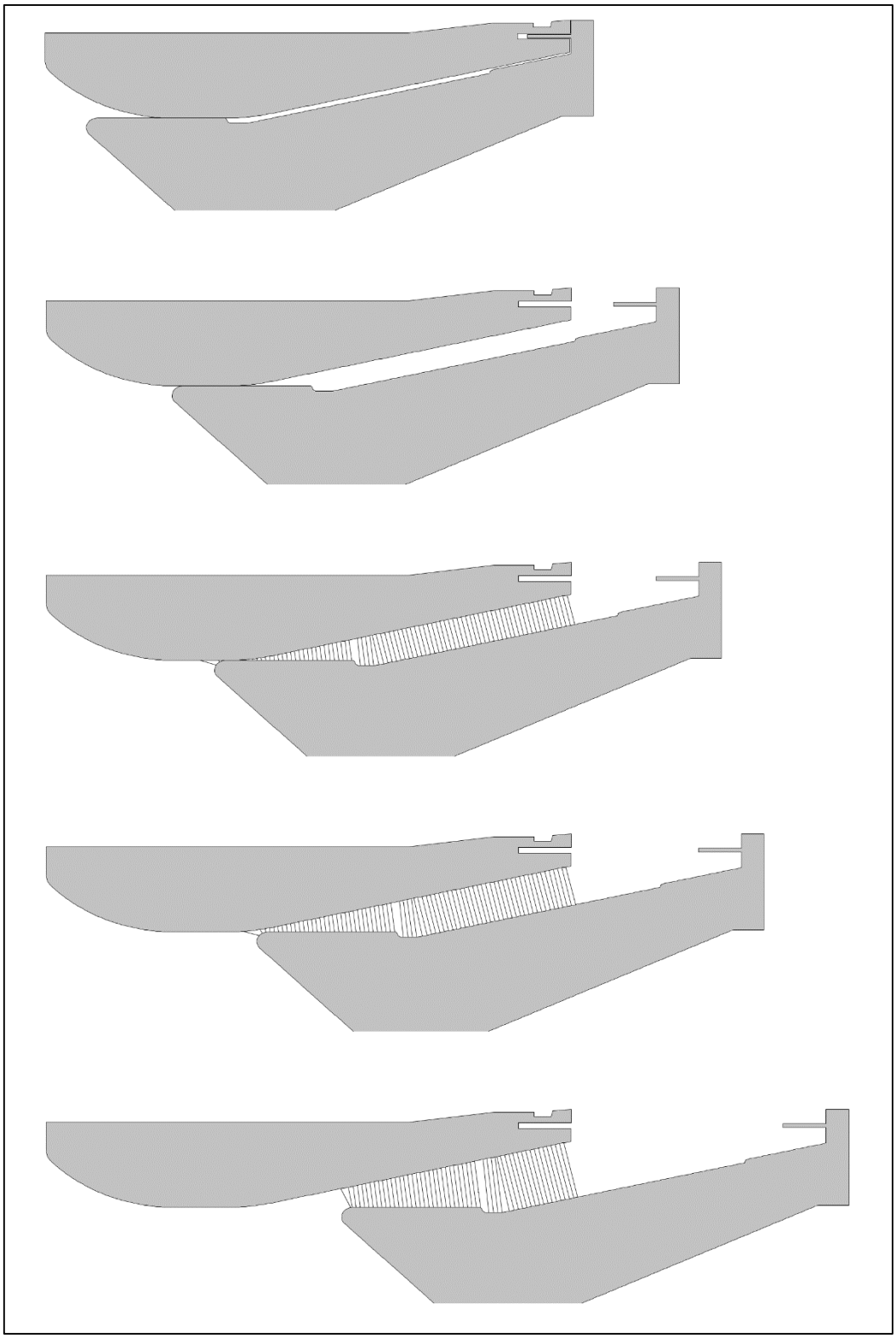

Figure 2.4. Calculated cross sections in the annular passage, taken from several nozzle positions

The angle of the normal vector of an individual cross section is calculated by considering the angles of the outer and inner surfaces bounding that cross section. This allows for the flow direction, which is dictated by the shape of the passage, being taken into account while calculating the area of each cross section, making sure that the cross sections are perpendicular to the assumed flow direction at every station on the length of the annular passage. Figure 2.5 illustrates the calculation method of the cross section boundaries and the normal angle, which are the parameters defining a cross section. For each station at the surface of the detachable nozzle, a point whose radial location is the average value of the inner surface radius and the outer surface radius, corresponding to the axial location of that station, is created. Following the assignment of that point, the normal angle, which is to determine the inclination of the cross section, is calculated. The inclination angle of the normal vector is set to the average value of the angles that the inner and outer surfaces make with the longitudinal axis, at the corresponding location. Once the root point and the inclination angle of the normal vector are calculated, a line which is perpendicular to the normal vector and which is passing through the root point is formed. Afterwards, the line is trimmed by the inner and outer surfaces in order to create a line segment that is bounded by the walls of the annular channel.

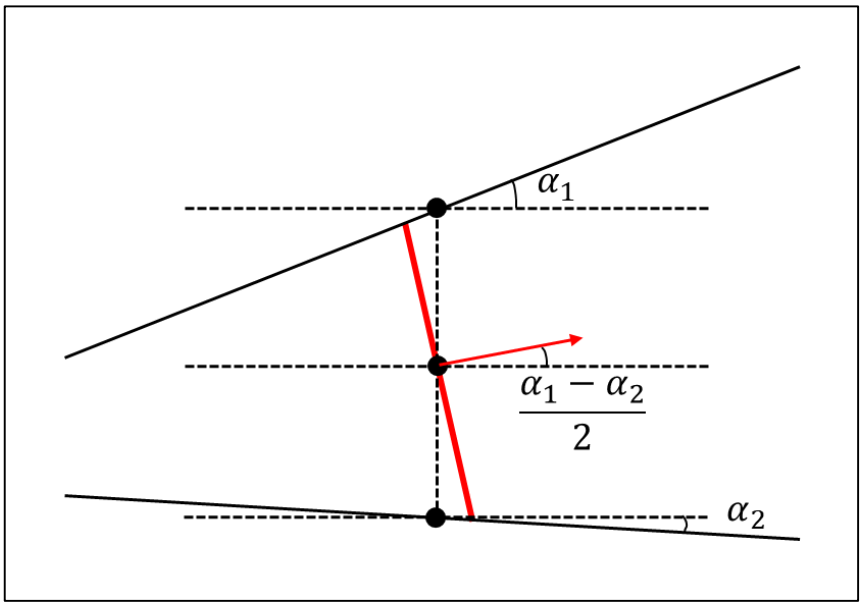

Figure 2.5. Calculation of the parameters of a single cross section in a flow passage

The calculations described above are performed at every station of the annular channel, creating multiple cross sections throughout the entire flow path, like the ones that are illustrated in Figure 2.4. After all the cross sections are calculated, the cross section which has the smallest area is designated as the throat section of the annular channel and its area is assigned as the throat area of the annular channel, to be used together with the throat area of the detachable nozzle in order to calculate the rate of the mass flow leaving the combustion chamber. The geometries that are shown in Figure 2.4 and Figure 2.5 are the side views of the flow fields, which are axially symmetric. The cross sectional areas are calculated by revolving the lines around the longitudinal axis. So, the area of a cross section should be regarded as the area of the side surface of a truncated cone.

In addition to obtaining the throat area of the annular channel, the cross sections are used for the purpose of calculating the pressure distribution around the detachable nozzle, which is in turn used in the calculation of the resultant force acting on it. For this purpose, the pressure distribution around the entire detachable nozzle has to be calculated.

For the resultant force calculation, the surface of the detachable nozzle is split into two sub-surfaces, which can be named as the inner surface and the outer surface, that are shown by the yellow and blue colored lines in Figure 2.6. The resultant force acting on each surface is obtained by first calculating the pressure at each point in the corresponding surface, and then taking the surface integral of pressure. Finally, the forces acting on the individual surfaces are summed in order to get the resultant force acting on the entire nozzle.

At the outer surface, the static pressure at each point is calculated using the cross section at that location. For the inner surface, there is no need for any cross section calculation, since the flow is assumed to be parallel to the longitudinal axis of the nozzle because of the symmetry in the flow path. Namely, the radial location of a point at the inner surface is already the radius of the cross section at that location.

So, the radius of a point at the inner surface can be used to calculate the cross sectional area of the flow at that location.

For the purpose of calculating the static pressure at a point in the outer surface or in the inner surface, Mach number at that location, which is calculated by (2.20), is used (Sutton & Biblarz, 2017).

$$\frac{A_{cs}}{A_t} = \frac{1}{M}\sqrt{\left(\frac{1+\frac{\gamma-1}{2}M^2}{\frac{\gamma+1}{2}}\right)^{\frac{\gamma+1}{\gamma-1}}} \qquad (2.20)$$

where M is the Mach number, A_{cs} is the cross sectional area at the corresponding point and A_t is the throat area of the annular channel if the point is at the outer surface. Else if the point is at the inner surface, A_t is the throat area of the detachable nozzle.

For each point, (2.20) is solved iteratively for M until the correct value of M, which results in the true value of $\frac{A_{cs}}{A_t}$ corresponding to that point, is reached when substituted in the equation. (2.20) is solved recursively for every point at the nozzle surface in order to find M. After the Mach number is calculated, the static pressure at each point is calculated via (2.21).

$$p = \frac{p_{total}}{\left(1+\frac{\gamma-1}{2}M^2\right)^{\frac{\gamma}{\gamma-1}}} \qquad (2.21)$$

Several assumptions regarding the flow inside the motor are made when calculating the pressure using (2.20) and (2.21), one of which is that the flow is chocked at the throat section of the annular channel and inside the detachable nozzle. The other assumptions are that the gasses behave as an ideal gas, and the flow is isentropic.

At each time step where the detachable nozzle is free to move, the resultant force acting on the nozzle is calculated via the procedure described above. After that, the acceleration of the nozzle is obtained by simply dividing the force by the nozzle

mass. Finally, the velocity and the position of the nozzle at the next time step is calculated by

$$\dot{x}^{n+1} = \dot{x}^n + \ddot{x}^n \Delta t \qquad (2.22)$$

$$x^{n+1} = x^n + \dot{x}^n \Delta t + \frac{1}{2}\ddot{x}^n \Delta t^2 \qquad (2.23)$$

where x is the position, $\dot{x}$ is the velocity and $\ddot{x}$ is the acceleration of the detachable nozzle, and Δt is the time increment between the current and next time step, which are denoted by the superscripts n and $n+1$, respectively.

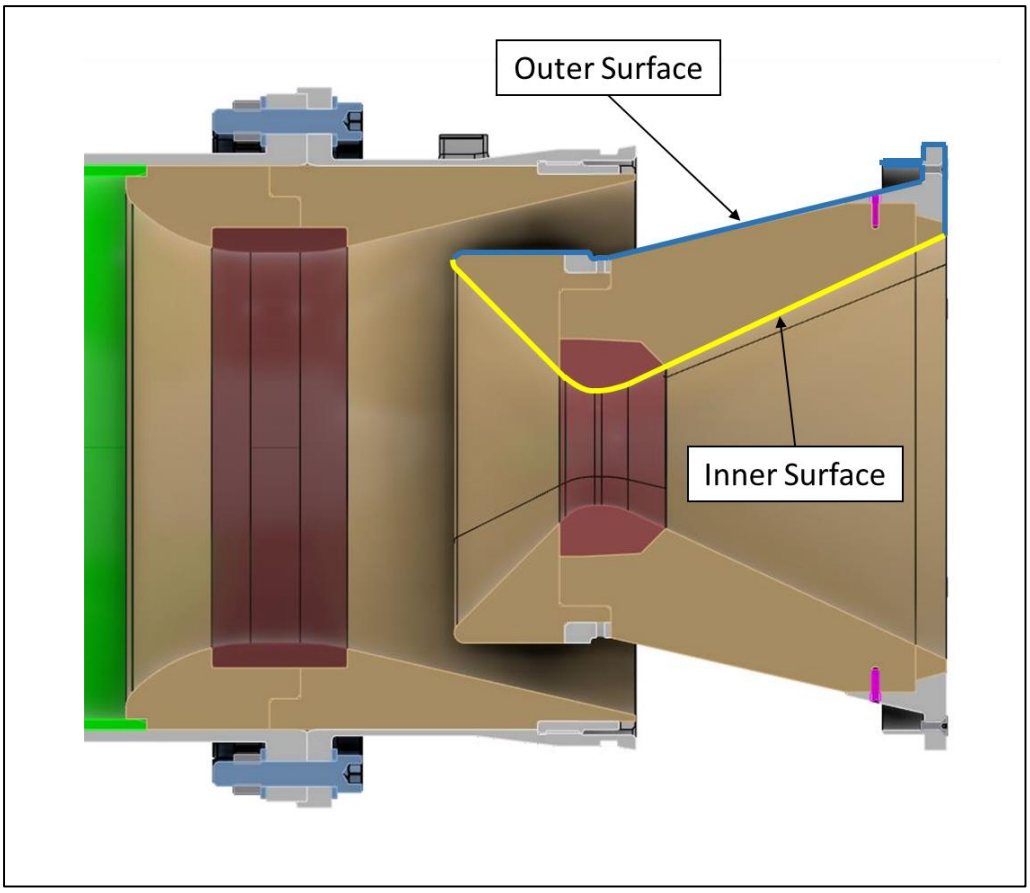

Figure 2.6. Visual representation of the two sub-surfaces of the detachable nozzle

2.2.4 Transient Propellant Burn Rate Calculation

As stated in the previous sections, (2.7) is used in order to calculate the time derivative of the chamber pressure and the pressure at the next time step. Following that, (2.8) is used for the purpose of calculating $\dot{m}_{in}$ that appears in (2.7), meaning that the propellant burn rate at a time step should be calculated in order to find the pressure at the next step.

In the normal operation phase where the transient parameters like chamber pressure and heat transfer rate to the propellant surface does not change very rapidly over time, the non-dimensional temperature distribution inside the thickness of the solid propellant grain can be treated as quasi-steady. So in the normal operation phase, the temperature inside the grain can be assumed to be a function of the spatial location and the propellant burn rate, for some predetermined initial temperature and propellant surface temperature values. This means that for this phase, the temperature distribution of the solid phase is not lagging when compared to the gas phase, since the pressure of the gas phase changes mildly with time. Hence at a time step, no additional heat will be transferred to the propellant in order to obtain the steady-state temperature distribution corresponding to that burn rate. As a consequence, the burn rate can be calculated by directly using the empirical relation that is relating the burn rate to the pressure, obtained by the test methods discussed earlier.

On the contrary to the steady phase, the assumption stated above does not hold for the thrust termination phase, where the pressure of the gas inside the chamber drops drastically over time, not allowing for the temperature distribution of the solid phase (propellant grain) to keep up. Therefore, in this steeply changing environment, the actual burn rate would be different from the burn rate that is measured in a constant pressure environment, even at the same instantaneous pressure. That is because the temperature distribution inside the propellant grain cannot reach its steady state value corresponding to that heat flux from the gasses, which is in turn related to that pressure level. Hence, in the termination phase, some additional part of the heat input

from the gas is spent on heating the solid and the actual burn rate turns out to be lower than its steady state value. The translation of this theory to a physical model that is based on the conservation equations, is discussed in the following section.

2.2.4.1 Physical Modeling of the Transient Burning Phenomenon in the Combustion Chamber

Before constructing the governing equations and listing the assumptions made in order to model the burnback of the propellant and the heat transfer from the gas phase to the propellant surface during rapid depressurization phase, it would be convenient to describe the process which is assumed to take place during the normal operation of the combustion chamber. Figure 2.7 illustrates the events occurring simultaneously during combustion. In this study, it is assumed that for a typical solid propellant burning environment, there is an infinitesimally thin solid phase reaction layer which is at the surface temperature that is constant and a propellant property. At this reacting surface, the contents of the solid propellant gasify through pyrolysis, thermal decomposition and dissociative sublimation. This unburned gas mixture then enters the gas phase reaction region and the combustion reactions between the gaseous reactants occur. In turn, the heat generated by this gas phase reactions is transferred to the propellant surface, providing the necessary heat feedback to the dissociation reactions of the solid phase, thus sustaining the combustion.

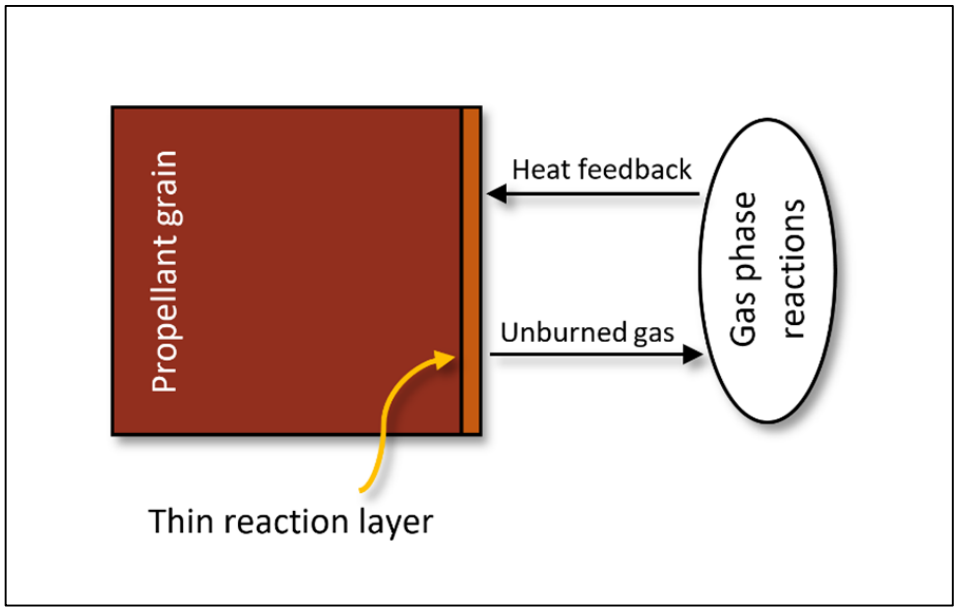

Figure 2.7. Simplified combustion environment

Assuming the heat transfer is one dimensional, the propellant thermal properties do not change with temperature and uniform throughout the grain, and no subsurface reactions occur in the propellant (Horton, Bruno & Graesser, 1968), one dimensional heat conduction equation inside the propellant grain can be written as

$$\frac{\partial T}{\partial t} = \alpha \frac{\partial^2 T}{\partial x^2} - r_b \frac{\partial T}{\partial x} \qquad (2.24)$$

where T is the temperature at a coordinate x inside the grain at time t, α is the thermal diffusivity of the propellant grain, and r_b is the burning rate of the propellant at any time instant. In (2.24), the origin of the coordinate system is attached to the retarding propellant surface.

At the normal operation phase where the nozzle detachment has not been initiated yet, the conditions are at steady state. So, $\frac{\partial T}{\partial t} = 0$. Hence for the normal operation phase, (2.24) becomes

$$\alpha \frac{\partial^2 T}{\partial x^2} - r_{b,steady} \frac{\partial T}{\partial x} = 0 \qquad (2.25)$$

where $r_{b,steady}$ is the steady burn rate which is calculated by the methods discussed earlier.

Assuming the propellant grain is semi-infinite and $T(-\infty) = T_0$ and $T(0) = T_s$ where T_0 is the initial conditioning temperature and T_s is the surface temperature of the propellant, (2.25) can be solved as

$$\frac{T - T_0}{T_s - T_0} = e^{\frac{rx}{\alpha}} \qquad (2.26)$$

From this point on, the term r is used instead of $r_{b,steady}$. (2.26) describes the temperature distribution inside the propellant grain at the normal operation phase.

In order to calculate the actual burning rate at the transient phase where significant changes in heat transfer to the propellant surface occur as a result of rapidly changing chamber pressure, $\frac{\partial T}{\partial t} \neq 0$ and (2.24) has to be solved for r_b. Since (2.24) is solved for the transient (thrust termination) phase, r_b term will present the unsteady burn rate $r_{b,unsteady}$, which is the actual burn rate of the propellant during this transient phase. So, for the thrust termination phase, (2.24) can be rewritten as

$$\frac{\partial T}{\partial t} = \alpha \frac{\partial^2 T}{\partial x^2} - r_{b,unsteady} \frac{\partial T}{\partial x} \qquad (2.27)$$

There are two unknowns ($T(x,t)$ and $r_{b,unsteady}$) in (2.27). So, another equation is needed to be solved for the both unknowns. For this purpose, (2.27) is accompanied by the equation governing the heat transfer to the propellant solid from the grain surface.

The equation for the heat transfer from the surface to the solid propellant, which is illustrated in Figure 2.8, can be written with the following form:

Heat transfer to the solid from the surface = Heat transfer to the surface - Heat required to gasify the solid.

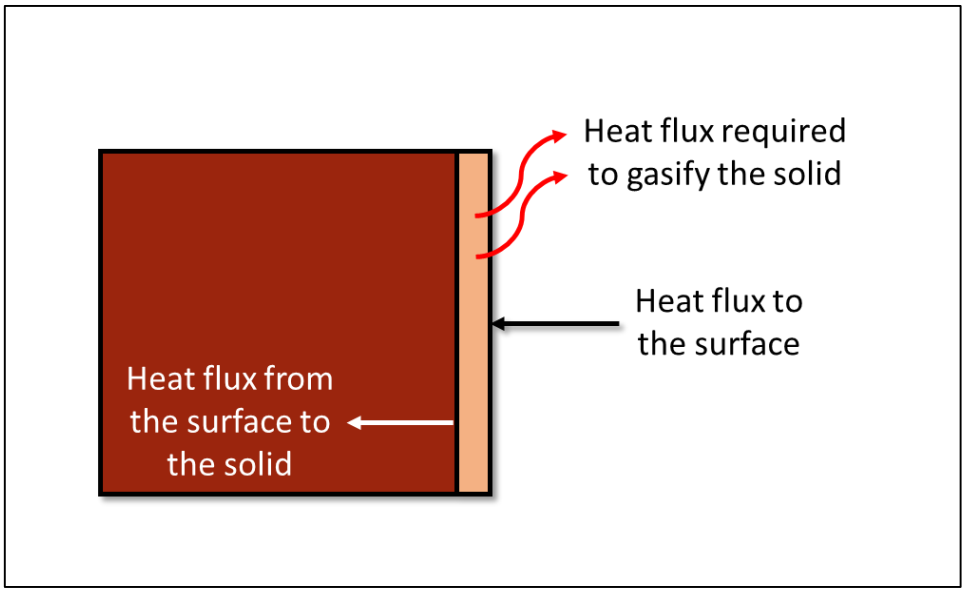

Figure 2.8. Energy balance at the propellant surface

The heat flux to the propellant solid from the surface, which is designated by q_1, can be formulated as

$$q_1 = k_P \left.\frac{\partial T}{\partial x}\right|_{x=0} \qquad (2.28)$$

where k_P is the thermal conductivity of the propellant.

The heat required to gasify the propellant, which is designated by q_2, can be written as

$$q_2 = \lambda \rho_P r_{b,unsteady} \qquad (2.29)$$

where λ is the propellant heat of gasification, which is the energy per mass required to gasify the propellant. Here, it is assumed that λ is a pressure independent constant. Subscript $unsteady$ is used here as in (2.27), because these equations are solved for the transient phase.

In order to derive an expression for the heat conducted to the propellant surface from the gas phase, another assumption, which is a consequence of the characteristic times of the solid and the gas phases, is made. As it was stated by Hart and McClure (1959),

for a typical combustion chamber environment, the characteristic time associated with the heat conduction from the gas phase to the solid is about an order of magnitude lower than the characteristic time associated with the heat conduction through the solid phase, meaning that the gas phase responds to the changes in the combustion chamber much more quickly compared to the solid phase. Hence, it is assumed that the heat transfer from the gas phase is not time dependent but it is pressure dependent.

The values of the steady state heat transfer rate from the gas phase to the surface of a propellant at different pressure values can readily be calculated using the steady state burn rate curve obtained from ultrasonic burn rate measurement devices, or from routine burn rate measurement test motors, etc. By any of the aforementioned methods, one obtains the $r_{b,steady}$ vs p data, which in turn can be used to calculate the heat transfer to the propellant surface which caused that value of $r_{b,steady}$. In other words, the heat transfer at a certain pressure can be known by the corresponding value of $r_{b,steady}$ at that pressure.

The heat transfer from the gas phase to the propellant surface, which is designated by q_3, can be formulated as

$$q_3 = r_{b,steady}\rho_P[\lambda + C_P(T_s - T_0)] \qquad (2.30)$$

where C_P is the heat capacity of the propellant.

The equation for the heat transfer from the propellant surface to the solid can be written as

$$q_1 = q_3 - q_2 \qquad (2.31)$$

Using r instead of $r_{b,steady}$ and $r_{unsteady}$ instead of $r_{b,unsteady}$, (2.31) can be rewritten as such:

$$k_P \left.\frac{\partial T}{\partial x}\right|_{x=0} = r\rho_P[\lambda + C_P(T_s - T_0)] - \lambda\rho_P r_{unsteady} \qquad (2.32)$$

Rearranging,

$$k_P \left.\frac{\partial T}{\partial x}\right|_{x=0} = \rho_P \lambda\left(r - r_{unsteady}\right) + r\rho_P C_P (T_s - T_0) \qquad (2.33)$$

Two equations (2.27) and (2.33) are established to solve for the two unknowns.

For the purpose of non-dimensionalization, the following relations are used:

$$\theta = \frac{T - T_0}{T_s - T_0} \qquad (2.34)$$

$$Y = \frac{r_0 x}{\alpha} \qquad (2.35)$$

$$\tau = \frac{r_0^2 t}{\alpha} \qquad (2.36)$$

$$R = \frac{r}{r_0} \qquad (2.37)$$

$$R_{unsteady} = \frac{r_{unsteady}}{r_0} \qquad (2.38)$$

$$F = \frac{\lambda}{C_P (T_s - T_0)} \qquad (2.39)$$

where r_0 is the steady-state burning rate of the propellant at the instant of termination initiation.

The non-dimensional form of the equations (2.27) and (2.33) are as follows (Horton, Bruno & Graesser, 1968):

$$\frac{\partial^2 \theta}{\partial Y^2} - R_{unsteady} \frac{\partial \theta}{\partial Y} = \frac{\partial \theta}{\partial \tau} \qquad (2.40)$$

$$\left.\frac{\partial \theta}{\partial Y}\right|_{Y=0} = R(1 + F) - R_{unsteady} F \qquad (2.41)$$

Boundary conditions:

$$\theta|_{Y=-\infty} = 0 \qquad (2.42)$$

$$\theta|_{Y=0} = 1 \tag{2.43}$$

Initial condition:

$$\theta|_{\tau=0} = e^{Y} \tag{2.44}$$

With these initial and boundary conditions, equations (2.40) and (2.41) are solved implicitly using backward time central space scheme. The discretized forms of the equations are written as

$$\frac{\theta_{i-1}^{n+1} - 2\theta_i^{n+1} + \theta_{i+1}^{n+1}}{\Delta Y^2} - R_{unsteady}^{n+1}\frac{\theta_{i+1}^{n+1} - \theta_{i-1}^{n+1}}{2\Delta Y} = \frac{\theta_i^{n+1} - \theta_i^{n}}{\Delta\tau} \tag{2.45}$$

$$\frac{\theta_1^{n+1} - \theta_{-1}^{n+1}}{2\Delta Y} = R^{n+1}(1+F) - R_{unsteady}^{n+1}F \tag{2.46}$$

Rearranging,

$$2(\theta_{i-1}^{n+1} - 2\theta_i^{n+1} + \theta_{i+1}^{n+1}) - \Delta Y R_{unsteady}^{n+1}(\theta_{i+1}^{n+1} - \theta_{i-1}^{n+1}) = \frac{2\Delta Y^2}{\Delta\tau}(\theta_i^{n+1} - \theta_i^{n}) \tag{2.47}$$

$$\theta_1^{n+1} - \theta_{-1}^{n+1} = 2\Delta Y R^{n+1}(1+F) - 2\Delta Y R_{unsteady}^{n+1}F \tag{2.48}$$

Introducing new coefficients for simplicity and rearranging (2.47),

$$(2+a)\theta_{i-1}^{n+1} - (4+2b)\theta_i^{n+1} + (2-a)\theta_{i+1}^{n+1} = -2b\theta_i^{n} \tag{2.49}$$

where $a = \Delta Y R_{unsteady}^{n+1}$ and $b = \frac{\Delta Y^2}{\Delta\tau}$

Introducing $c = \Delta Y R^{n+1}$ to (2.48),

$$\theta_1^{n+1} - \theta_{-1}^{n+1} = 2c(1+F) - 2aF \tag{2.50}$$

The solution domain, which extends over the web of the solid propellant grain, is discretized as shown in Figure 2.9.

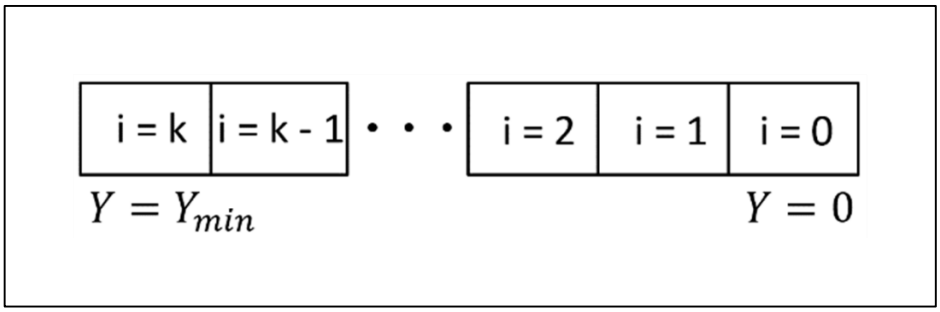

Figure 2.9. Discretization of the grain

The absolute value of Y_{min} should be large enough so that the semi-infinite propellant assumption is imposed to the domain. In addition, $\Delta\tau$ should be small enough in order to ensure time accuracy.

For i = 0, (2.49) reduces to

$$(2+a)\theta_{-1}^{n+1} + (2-a)\theta_1^{n+1} = 4 \qquad (2.51)$$

Inserting (2.50) into (2.51) and rearranging,

$$a[F(2+a-c)-c] + 2\theta_1^{n+1} = 2 + 2c(1+F) \qquad (2.52)$$

For i = 1, (2.49) can be written as

$$a - (4+2b)\theta_1^{n+1} + (2-a)\theta_2^{n+1} = -2 - 2b\theta_1^n \qquad (2.53)$$

For i = 2 to k – 2,

$$(2+a)\theta_{i-1}^{n+1} - (4+2b)\theta_i^{n+1} + (2-a)\theta_{i+1}^{n+1} = -2b\theta_i^n \qquad (2.54)$$

For i = k - 1,

$$(2+a)\theta_{k-2}^{n+1} - (4+2b)\theta_{k-1}^{n+1} = -2b\theta_{k-1}^n \qquad (2.55)$$

Equations (2.52), (2.53), (2.54) and (2.55) constitutes a system of k equations, which can be solved as a tridiagonal system for k unknowns (k–1 unknowns in the θ field and 1 unknown which is a). The tridiagonal system of equations can be written as such:

$$\begin{bmatrix} F(2+a-c)-c & 2 & 0 & \dots & \dots & \dots & 0 \\ 1 & -(4+2b) & 2-a & 0 & \dots & \dots & 0 \\ 0 & 2+a & -(4+2b) & 2-a & 0 & \dots & 0 \\ \vdots & \ddots & \ddots & \ddots & \ddots & \ddots & \vdots \\ 0 & \dots & 0 & 2+a & -(4+2b) & 2-a & 0 \\ 0 & \dots & \dots & 0 & 2+a & -(4+2b) & 2-a \\ 0 & \dots & \dots & \dots & 0 & 2+a & -(4+2b) \end{bmatrix} \begin{bmatrix} a \\ \theta_1^{n+1} \\ \vdots \\ \vdots \\ \vdots \\ \vdots \\ \theta_{k-1}^{n+1} \end{bmatrix} = \begin{bmatrix} 2+2c(1+F) \\ -2-2b\theta_1^n \\ -2b\theta_2^n \\ \vdots \\ \vdots \\ \vdots \\ -2b\theta_{k-1}^n \end{bmatrix} \quad (2.56)$$

In the system of (2.56), the unknown a appears in the coefficient matrix too. So, a solution to the system cannot be obtained right away. For this reason, an iterative solution is employed. The system of equations is solved with an initial value of a and a corrector value of a is produced by the solution. Then the corrector value of a is substituted into the system recursively to be the predictor of the new solution until a convergence is obtained between the predictor and the corrector values of a.

The pressure at the current time step is known since it is calculated using the derivative of the pressure at the previous time step. So, the parameter R^{n+1} is already known and can be used to calculate the parameter a and $R_{unsteady}^{n+1}$. Hence, the actual burn rate $r_{unsteady}$ can be found at the current time step, which is in turn going to be used to calculate the chamber pressure at the next time step.

2.2.4.2 Calculation of the Heat of Gasification and the Surface Temperature of the Propellant

In order to solve for the temperature distribution inside the propellant grain and the instantaneous burn rate for each time instant at the rapid depressurization phase, the surface temperature and the heat of gasification of the propellant, which require procedures that are more cumbersome in order to be measured, have to be known. Since measuring these two parameters is a formidable task, they are calculated using

some of the known attributes of the propellant. For the purpose of calculating the surface temperature of the propellant, which is assumed to be constant during the entire burn, the propellant surface temperature calculation method that is described by Lenoir & Robillard (1957) is used on the propellant of the present study.

The heat of gasification of the propellant (λ) is calculated using a simplistic approach that is devised for this study, where λ is calculated with respect to the enthalpies of the reactions, each of which corresponds to the heat required to gasify an individual component in the propellant formulation.

The propellant is assumed homogenous with respect to the ratio of the components in the propellant formulation, i. e. the propellant has the same mixture of components everywhere in the solid. In this study, the test motor that is used to validate the solver burns a non-aluminized propellant, which consists mainly of AP and HTPB. So, a simple method that utilizes the reaction enthalpies and mass fractions of different components in the propellant unit mass is employed to calculate the heat required to gasify the unit mass of the solid propellant and is described by (2.57).

$$\lambda = m_1 \Delta H_1 + m_2 \Delta H_2 + \cdots + m_i \Delta H_i \qquad (2.57)$$

where m_i denotes the mass fraction of the i^{th} component and ΔH_i denotes the heat released or absorbed per unit mass of the i^{th} component entering the corresponding dissociation reaction. Since the propellant used for this study is treated to consist mainly of AP and HTPB, the heat required to decompose the unit mass of AP with its mass fraction and the net heat required for the pyrolysis of HTPB with its mass fraction are used in (2.57) to compute λ. Sum of the mass fractions have to equal 1 for the calculations to be physically sane.

2.2.5 Thrust Calculation

The thrust that the motor produces is calculated with different approaches at different phases. In the normal operation phase, where the detachable nozzle is connected to the motor, the thrust is calculated for each time instant using (2.58) (Sutton &

Biblarz, 2017), where A_t denotes the detachable nozzle throat area, p_e and A_e denote the pressure and the cross sectional area at the detachable nozzle exit section respectively.

$$Thrust = p_c A_t \sqrt{\frac{2\gamma^2}{\gamma-1}\left(\frac{2}{\gamma+1}\right)^{\frac{\gamma+1}{\gamma-1}}\left(1-\left(\frac{p_e}{p_c}\right)^{\frac{\gamma-1}{\gamma}}\right)} + (p_e - p_{amb})A_e \quad (2.58)$$

At the thrust termination phase, which starts when the physical connection of the detachable nozzle to the remaining motor is terminated, the thrust is calculated by integrating the pressure at the whole inner surface of the motor, which consists of the outer nozzle surface and the combustion chamber surface. Since the detachable nozzle is not able to transfer any force that is acting on it to the motor at this phase, the thrust that the motor produces is caused by the resultant force that is generated by the gas pressure acting on the outer nozzle and on the combustion chamber surfaces.

The pressure distribution acting on the outer nozzle is calculated using the cross sections in the annular channel and integrated to find the force acting on the outer nozzle, then it is summed with the resultant force acting on the combustion chamber at each time instant at the termination phase in order to compute the thrust. For the outer nozzle surface, the pressure is assumed to be equal to p_c at the points before the starting point of the cross sections, and the pressure is assumed p_c for the whole surface of the combustion chamber. In the end, the pressure at every point in the motor is known and can be used in the surface integration.

CHAPTER 3

RESULTS AND DISCUSSION

For the purpose of validating the solver that is developed for this study, a test motor with an end burning propellant and a detachable nozzle was manufactured and fired multiple times. At each firing, the chamber pressure of the motor was set to a different constant value. In order to obtain a different chamber pressure level, a nozzle throat insert with a different inner diameter was mounted to the throat section of the detachable nozzle for each firing.

For each test, after a test motor started its normal operation phase and reached its operating chamber pressure, the holding mechanism, which keeps the nozzle from being ejected by means of the inner pressure, was released at a predetermined time instant and the pressure and thrust histories of the test motors were recorded from the beginning of the operation to the end of the pressure discharge.

3.1 Properties of the Thrust Termination Test Motor

An end burning propellant was used in the test motors in order to obtain a constant operating pressure at the normal operation phase. For an end burning configuration, the area of the burning surface of the propellant remains constant while the motor operates, because the geometry becomes essentially a circular cylinder whose surfaces are sealed except its one circular end, which is free to burn. Since the burning surface moves normal to itself while the burn continues, the length of the propellant cylinder decreases as the its area of the burning end remains constant. As a consequence, the burn area does not change in time. In turn, the rate of the mass flow entering and leaving the combustion chamber converges to some constant values and a constant chamber pressure is reached. This holds for a motor whose nozzle throat area does not change throughout the operation, which can be a diameter

increase caused by chemical erosion, or a diameter decrease caused by the agglomeration of condensed phase particles in the throat section. Figure 3.1 illustrates the burning surface of the propellant and the sealed surfaces, burning surface being the one at the right end, and the sealed ones being the side surface (the one that is adjacent to the motor case wall) and the base surface (the surface that is at the left end of the propellant grain).

Figure 3.1 also demonstrates the geometry of the test motor at three different stages of the operation. Some time after ignition, when the motor is operating steadily with a constant chamber pressure, the detachment mechanism is invoked manually and the detachable nozzle starts its motion away from the motor. After a short while, the nozzle leaves the motor entirely and creates the discharge area which is named as outer nozzle throat. Since the cross sectional area of the outer nozzle throat is drammatically larger than that of the detachable nozzle throat, a sudden depressurization is observed.

A non-aluminized propellant formulation, which is composed mainly of Ammonium Perchlorate as the oxidizer and HTPB (Hydroxyl Terminated Polybutadiene) as the binder was used in the test motors. Additionally, the propellant side surface that is discussed above was kept from burning by applying inhibitors, which stick to the surface and seals it from the combustion environment.

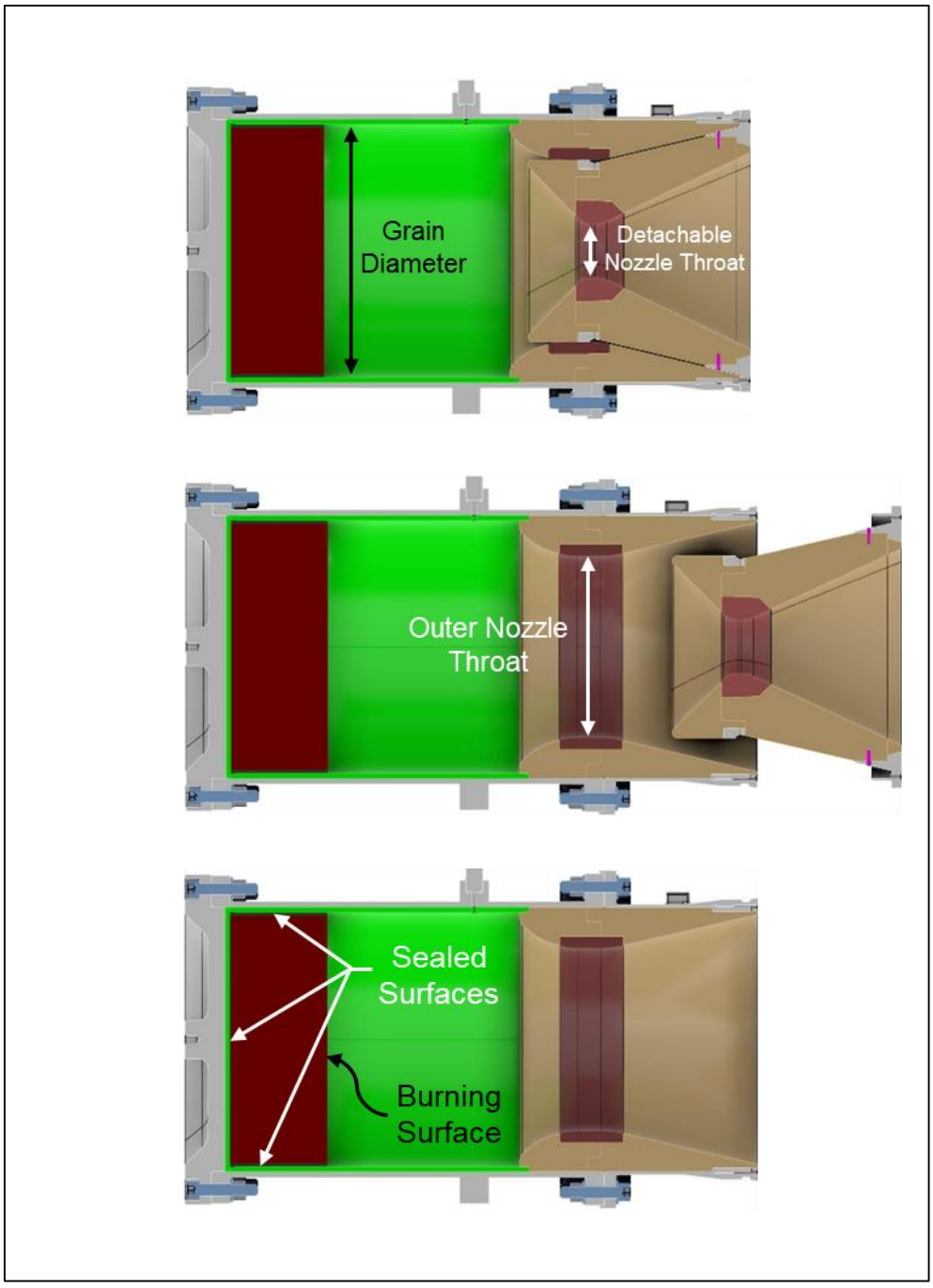

Figure 3.1. Side-view of the test motor at three different time instants

3.2 Testing Methodology and Instrumentation

In order to test the performance of a rocket motor by measuring the parameters like chamber pressure and thrust histories during the firing, the motor needs to be constrained in every axis, making sure that the motor remains stationary during the test. If the thrust output is to be measured, an appropriate load cell should be positioned at every joint linking the motor to a rigid structure in the axis of measurement. Additionally, appropriate pressure measurement holes and pressure sensors should be located on the motor, at the locations of interest where the pressure history is sought. Other outputs such as the temperature at the outer surfaces, vibration, noise, strain, etc. are also some of the important parameters that are measured frequently. In the case of the present study, the pressure and thrust histories obtained from the tests are of particular interest, since they are the parameters that are aimed to be estimated correctly. Therefore, they were acquired in the tests and are reported herein.

The instruments that are used on the test motors for the purpose of data acquisition are illustrated in Figure 3.2, and a sketch, which illustrates the general aspects of the test site is given in Figure 3.3. The tests are conducted in open air conditions, where the ambient pressure is about 12.9 psi. The motors are constrained by a solid wall on the thrust axis and by a frame on the other axes. The frame is free to move axially on the lubricated rails so that it would carry the lateral loads only, preventing the frame from taking any axial force, which would cause errors in thrust measurements.

A load cell, which has a load limit of approximately 250 kN is attached to the head end of the motor with bolted connections. The capacity of the load cell is several orders of magnitude higher than the thrust output of the motors at the normal operation phase. This type of load cell is chosen in order to protect the load cell from the possibility of an unexpectedly high thrust level, which might occur at the detachment phase. The load cell itself is attached to an interface, which touches the thrust block (solid wall) without any bolted connection. As the thrust is generated, the motor pushes the load cell towards the wall and that force measured by the load

cell is designated as the thrust. In the other axes, the motors are secured by a frame, in a way that no force is transferred by the motors to the frame in the thrust axis.

The chamber pressure is measured from a single hole that is drilled in the motor case. For backup purposes, two pressure sensors are attached to an apparatus, which is in turn attached to this hole with leak proof connections. The pressure sensors that are used for the data acquisition have 500 psi of maximum pressure measurement capability.

Since the detachment and extinguishment are expected to occur in a time interval that is on the order of milliseconds and sharp changes in pressure and thrust histories of the motors in the thrust termination phase are expected, sampling frequency should be large enough for both pressure and thrust data. For this reason, thrust and pressure are sampled with a frequency of 8 kHz.

The load cell and the pressure transducers that are used in the tests are of strain gauge type. Since the load capacities of the sensors can be considered to be high compared to the loads that are expected to occur in the tests, care is given to the calibration of the sensors, ensuring that the linearity of the measurement is not compromised for small values of pressure and thrust.

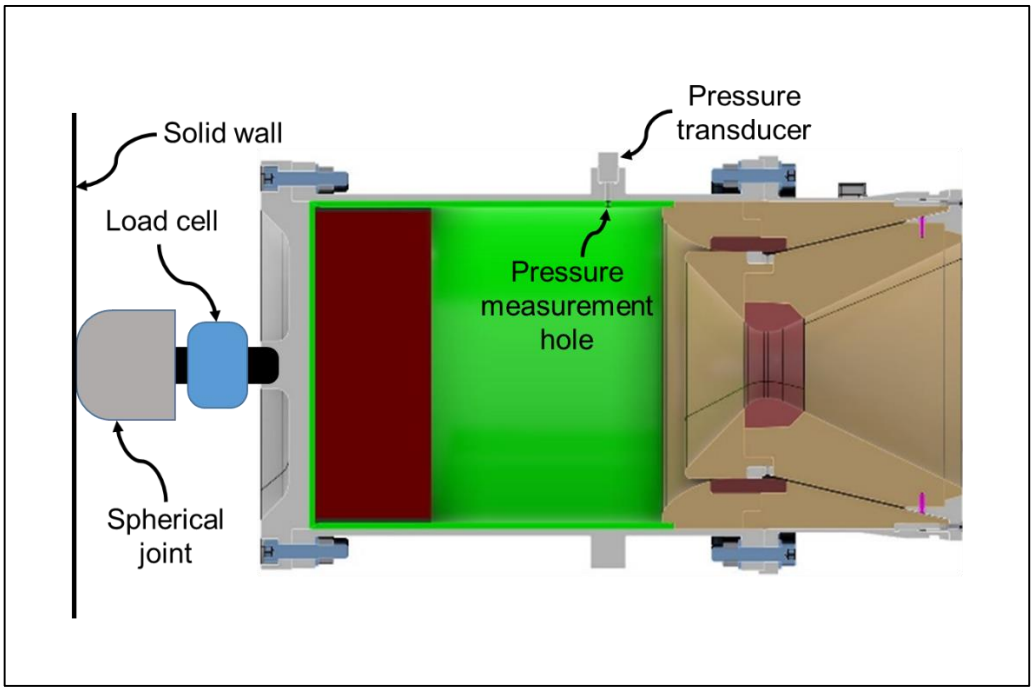

Figure 3.2. Instrumentation of the test motors

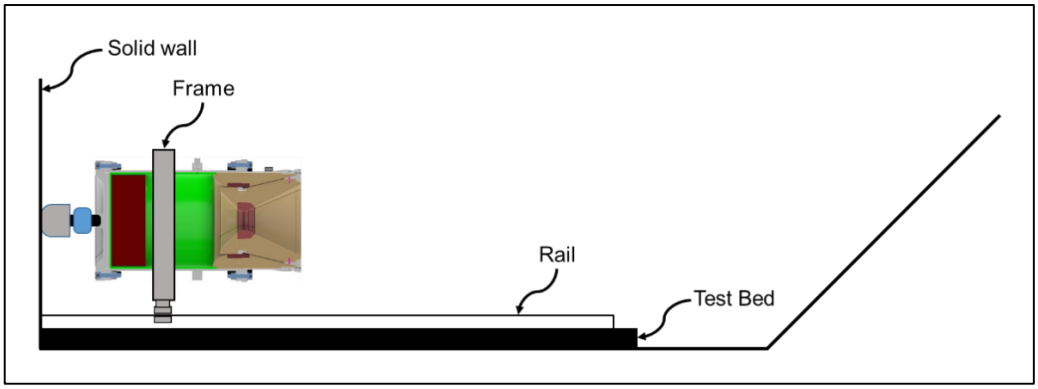

Figure 3.3. Illustration of the test motor secured to the test bed

3.3 Qualitative Results of the Termination Tests

Two tests were performed, each having a different level of operating pressure. The same propellant formulation and the same motor geometry were used for the test motors, detachable nozzle throat areas being the only difference between the tests. In addition, both motors were conditioned to 21°C before the tests. The goals of the test firings were to verify that the propellant extinguishment and thrust termination

occurs as estimated by the unsteady burn rate model, to test the competence of the solver in capturing the transient behavior of the pressure vs. time curve at the thrust termination phase, and to test the ability to predict the thrust that the motor generates after the detachment initiation at different operating pressures.

During each static firing test, the sequence of detachment, the plume of the motor after detachment and the motion of the detachable nozzle were captured using a high speed camera. Figure 3.4 summarizes the sequential events taking place during the nozzle detachment in one of the tests. For the both firings, similar scenarios were encountered in terms of nozzle separation and plume behavior. Hence, the snapshots taken from one of the tests are shown.

Shortly after the detachment mechanism is invoked, detachable nozzle becomes free and starts its motion away from the motor. Up to some point, the annular channel around the detachable nozzle remains obstructed. After the detachable nozzle passes a certain location inside the outer nozzle, the gasses start to rush through the annular channel, which is no longer blocked by the outer diameter of the detachable nozzle, as it is observed in the second image of Figure 3.4. This behavior is also calculated by the solver and can be observed in Figure 2.4. Detachable nozzle continues its motion by means of the inner pressure. In the meantime, pressure gets rapidly discharged because of the continuously enlarging annular channel. At some point, the plume becomes noticeably weak, especially when the detachable nozzle is ejected completely, as it can be seen in the third image of Figure 3.4. Finally, the plume disappears completely, indicating that the propellant is extinguished and the thrust is terminated, which is observed in the fourth and fifth images.

After the static firings, the motors were disassembled for inspection. Figure 3.5 shows the propellant sub-assembly of a test motor before and after the firing, which is the part also seen in Figure 3.1 from the side view. In the first image of Figure 3.5, the initial burning surface (black) and the inhibitor surface (white) surrounding the propellant grain can be seen. In the second image, one can observe that the propellant has burnt in the normal direction to the burning surface (downwards in the image),

leaving the inhibitor unburnt. In addition, it can be seen that the majority of the propellant has remained without burning after termination. Finally, it is observed that the extinguishment has left a nearly flat surface, meaning that the whole surface ceased to burn roughly at the same time.

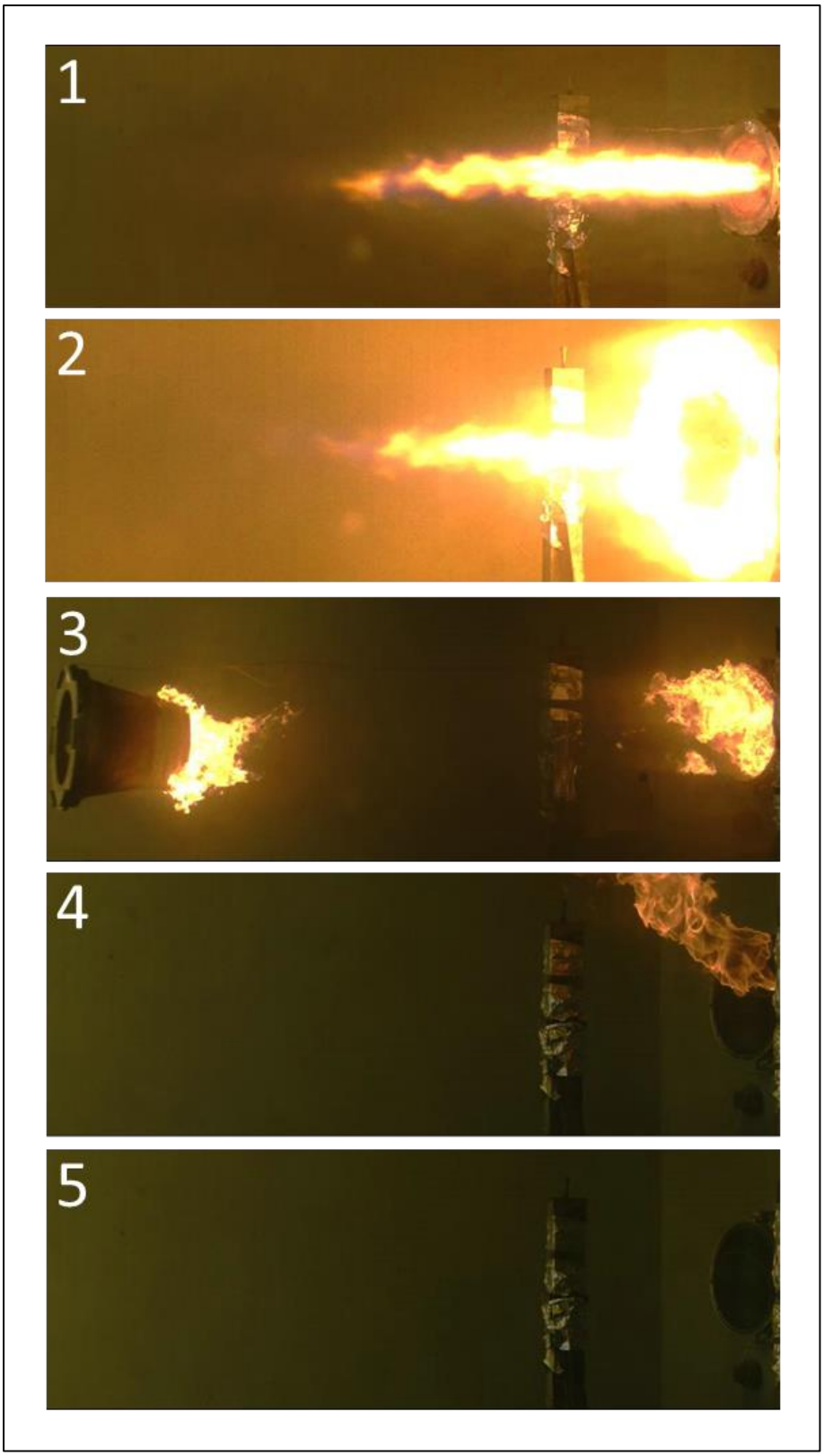

Figure 3.4. Thrust termination sequence of a test motor

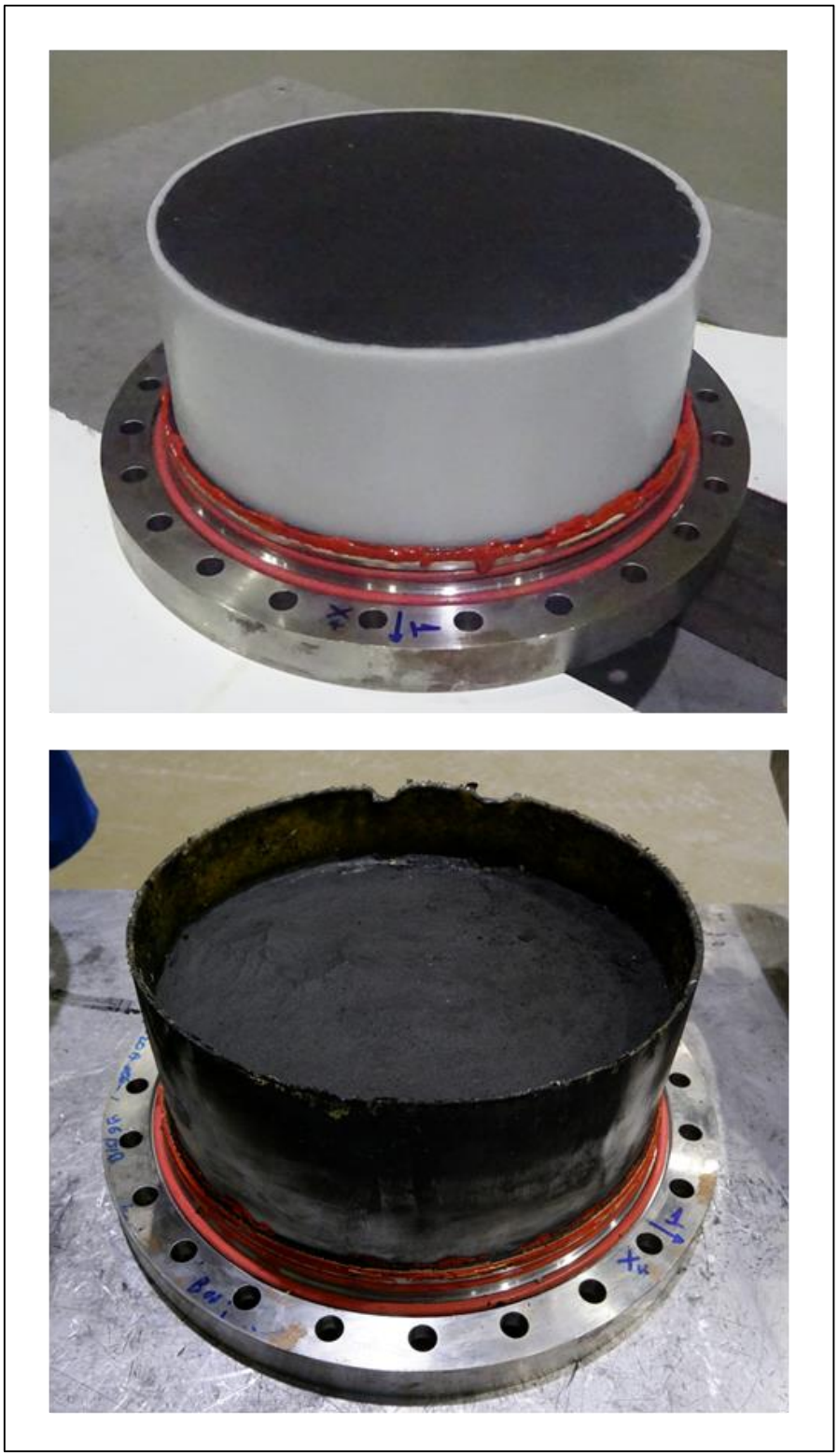

Figure 3.5. The propellant grain before and after the static firing

3.4 Comparison Between the Static Firing and the Solver Results

The propellant and chamber properties, detachment time, the geometry of the detachable nozzle and the geometry of the nozzle section of the motor that is obtained after detachment were input to the solver in order to model the test motors and the simulation results were obtained for each firing.

The throat diameters, which are non-dimensionalized with respect to the propellant grain diameter and the corresponding motor operating pressures of the two test motors are summarized in Table 3.1.

Table 3.1 Properties of the test motors (detachable nozzle and outer nozzle throat diameters non-dimensionalized w.r.t. the propellant grain diameter)

	Detachable Nozzle Throat Diameter	*Outer Nozzle Throat Diameter*	*Operating Pressure [MPa]*
Test Motor 1	0.09	0.7	1.10
Test Motor 2	0.08	0.7	1.98

Pressure-time and thrust-time outputs from the static firings are compared to the results obtained from the solver estimation of the corresponding firing. The exact value of the time at the detachment signal is obtained from the pressure history of the test motor by pin pointing the instant at the pressure drop. The corresponding detachment time is in turn input to the solver in order to simulate the test properly.

3.4.1 Comparison of the Pressure vs. Time Curves

Comparison of the entire pressure vs. time history of the firings with the solver results are shown in Figure 3.6. As it is discussed in the previous sections, a constant operating pressure has been achieved by the usage of an end burning propellant. Following propellant ignition, the combustion chamber gets pressurized by the mass flow into the combustion chamber, and the pressure reaches its steady value when a

balance is found between the mass flow into and out of the chamber. Finally, the chamber pressure drops drastically when the nozzle is detached.

It can be observed that due to the igniter operation, there is a high pressure peak relative to the operation pressure of the first test motor, which is not modeled by the solver. In addition, there is a relatively long transition phase before the operation pressure is reached for the both firings, which cannot be captured by the solver. The reason behind this difference between the solver output and the test result can be attributed to the inhomogeneity caused by the curing process at the manufacturing of the propellant, meaning that the region close to the surface of the propellant might not have the same properties with the remaining of the propellant, causing low burn rate at this region. That is of the possible scenarios that might be causing this difference and more studies on this propellant should be conducted in order to reach to a decisive answer. Since the focus of this study is to capture the performance in the termination phase, improvements in the solver to capture this area can be considered as a future enhancement effort.

Focusing on the sudden pressure drop at approximately 6.5 s after ignition for Test 1, and 9.3 s after ignition for Test 2, it can be observed that the chamber pressure drops to ambient pressure (≈0.09 MPa), indicating that the thrust is terminated.

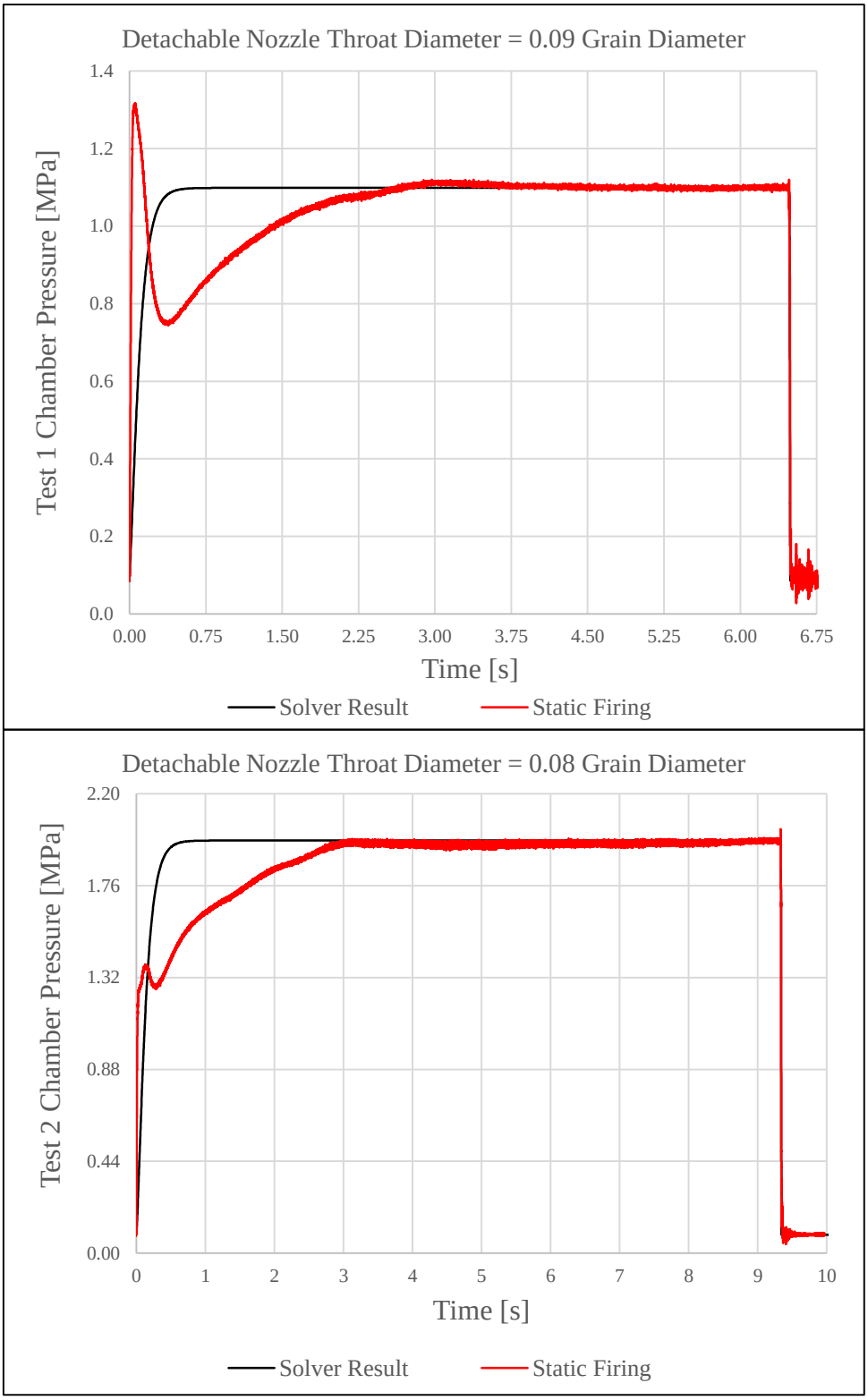

Figure 3.6. Pressure vs. time curves of the entire firing intervals for Test 1 & 2

In order to assess the ability of the solver to capture the pressure transient during rapid depressurization, attention is given to the termination phase, which lasts for approximately 20 ms for Test 1 and 10 ms for Test 2. Figure 3.7 shows the pressure vs. time curves produced by the solver and produced by the firings in a narrower focus. Right after detachment, starting from approximately 6.48 s for Test 1 and 9.33 s for Test 2, there is a relatively mild drop in the pressure before the steep pressure decrease, which is due to the increase in the internal motor volume while the detachable nozzle is being ejected from the motor. This is the phase in which the detachable nozzle starts its movement but the annular channel has not been opened to the atmosphere yet. After some point, secondary annular discharge area appears as the nozzle moves further and a steep drop in the pressure is observed. This is the phase in which the time derivative of the pressure becomes significant and the transient burn rate, which is calculated for a time instant, differs from the steady burn rate. For this case, this steep pressure drop causes the unsteady burn rate to reach zero at some point and in turn extinguish the propellant. By comparing the pressure vs. time curves, it can be concluded that the ballistic solver estimates the pressure profile with a satisfactory accuracy.

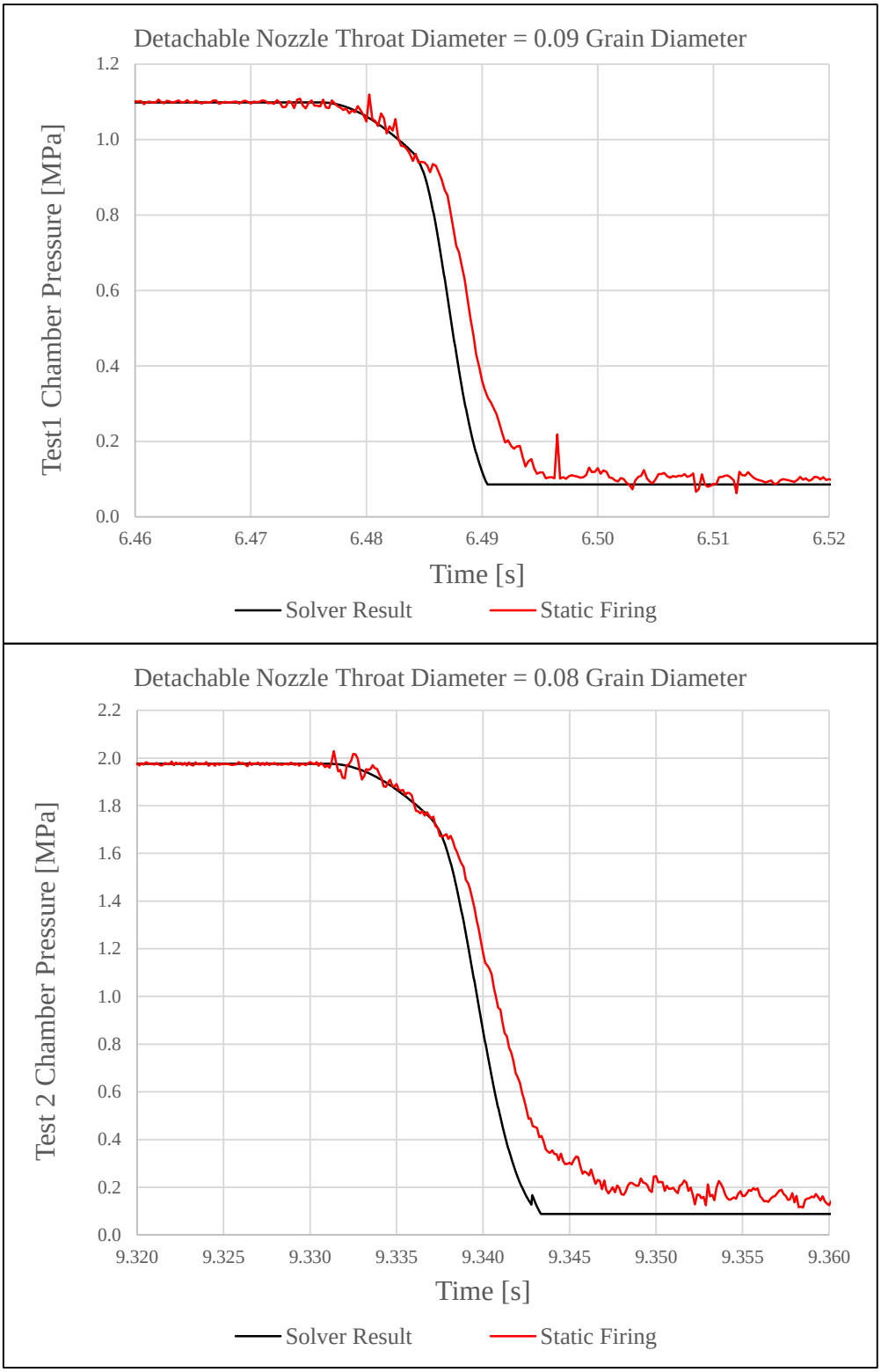

Figure 3.7. Pressure vs. time curve focused on the termination phase for Test 1 & 2

3.4.2 Comparison of the Thrust vs. Time Curves

During the normal operation phase, the forces on the nozzle act in the opposite direction to the thrust vector, contributing negatively to the resultant thrust force. When the nozzle is detached from the motor, since the nozzle is no longer connected, the negative effect of the forces on the nozzle suddenly disappear on the system while the chamber pressure is still large. So, one can expect a sudden peak in the thrust at the instant of detachment, fading as the pressure decreases.

For a time instant, the solver calculates the force on the detachable nozzle and on the outer nozzle by calculating the surface integral of pressure using the methodology that is discussed at the previous sections. Then it uses the force on the detachable nozzle to calculate its position in the next time instant, and it uses the force on the outer nozzle surface in order to use it for the calculation of the resultant force acting on the inner surfaces of the motor to calculate the total thrust at the termination phase.

Figure 3.8 illustrates the thrust vs. time curves obtained by the solver and the ones produced by the static firings. The thrust values are non-dimensionalized with respect to the nominal thrust produced by the corresponding test motor before the detachment. Observing Figure 3.8, the ballistic solver calculates a peak at the instant of detachment. Since the force on the outer nozzle and hence the thrust is calculated by the pressure distribution obtained by using the isentropic equation and the chamber pressure as the stagnation pressure, the thrust gradually decreases while the pressure drops as the nozzle moves further away, reaching zero when the pressure reaches ambient.

In the actual thrust history of the firing, one can see sudden peaks, which cannot be captured by the solver. At first, it is questioned if the reason behind the oscillating behavior of the thrust profile was the unsteady oscillations of the pressure waves going back and forth inside the motor, resulting from the sudden expansion caused by detachment. In order to test the possible cause, a RANS based transient CFD simulation is performed, in which the detachable nozzle is allowed to move in one

axis and away from the motor by means of the chamber pressure. Fluent® 2020R1 is employed in the simulation of the flow and nozzle motion, using a dynamic mesh with the overset mesh technique. The domain is discretized as two cell zones, one cell zone being the flow field around the detachable nozzle, which can move axially, and the other one being the flow field inside the motor, first one overlapping the second one. Because of the limitations of the overset mesh method, the simulation is started from the position of the nozzle where the annular channel is opened for the first time. The transient solution is initialized by solving for the flow and making the flow variables converge, applying the boundary conditions like the mass flow rate into the combustion chamber at the initial condition where the nozzle is in the mentioned position. After the flow variables converge for that position, the nozzle is allowed to move and the flow variables are calculated while the position of the nozzle being updated for every time step while the transient simulation proceeds.

Figure 3.9 shows the thrust history that is calculated by the CFD simulation for the time period starting from the time instant when the nozzle is in a position at which the annular channel is opened for the first time, to a time instant that is far enough in order to achieve zero thrust at the end. In addition, the results of the present study for the same time interval is plotted together with the CFD results in order to compare the two solutions. CFD simulation is performed for Test 2. Figure shows that some oscillations in thrust, which are caused by the transient behavior of the fluid at the depressurization phase, are captured using RANS equations, while the magnitude of these oscillations are minor compared to the magnitude of the oscillations that are observed in Figure 3.8. Moreover, the thrust values calculated by the CFD simulation over time are in close agreement with the values calculated by the solver of the present study. So, the comparison of the two results suggests that while affecting the thrust profile, the waves inside the combustion chamber that are formed by the sudden expansion are not the leading cause of the sudden peaks and valleys in the thrust profile of the motors in these two tests.

After some additional considerations and in light of these findings, the sudden peaks and drops in the thrust curve that are encountered after detachment are attributed to

the elastic behavior of the motor structure. While the motor is in the normal operation phase, the pressure distribution inside the motor strains the structure like a pressure vessel, and the motor becomes loaded like a spring. When the nozzle is detached, the forces that were being exerted on it in the normal operation phase are no longer transferred to the motor case. This phenomenon can be thought as a process which is analogous to releasing a preloaded spring. The energy that is stored in the strained motor case is released and makes the waves that are seen in Figure 3.8, just like the waves that can be observed in a spring mass damper system. After a while, the thrust reaches zero and stays constant at that value, because the thrust is measured by a load cell that is in front of the motor and is not connected to the wall with bolted connections. Once the force exerted on the load cell reaches a negative value, the load cell ceases to touch the wall and outputs zero value from that point. The load cell should be connected with bolted connections in order to measure negative values, which is expected to happen because of the spring behavior. In order to model this phenomenon, it is planned to solve for the elastic behavior of the motor and compare the results with the test firings as a future work in order to come to a decisive conclusion.

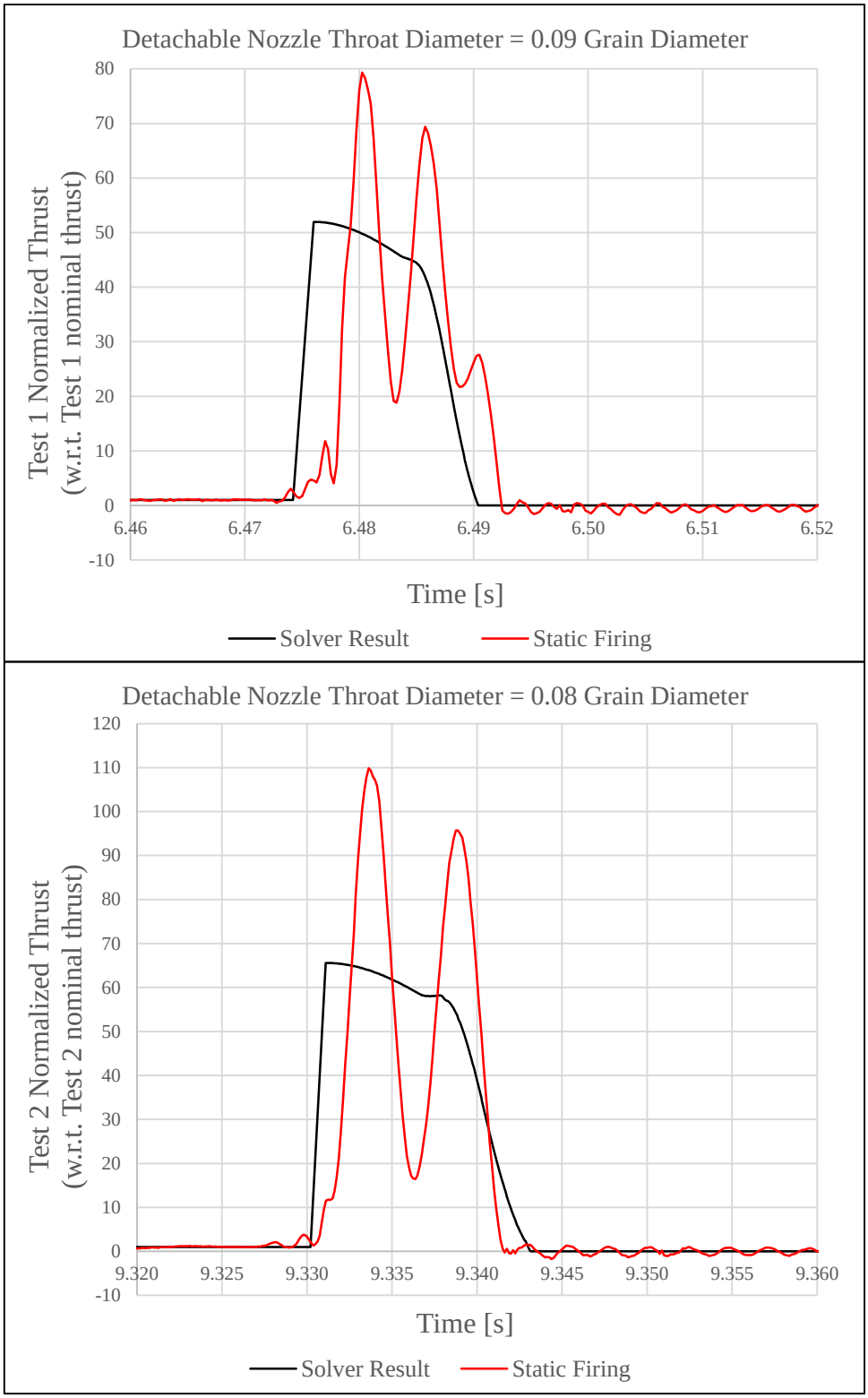

Figure 3.8. Thrust vs. time curves focused on the termination phases for Test 1 & 2

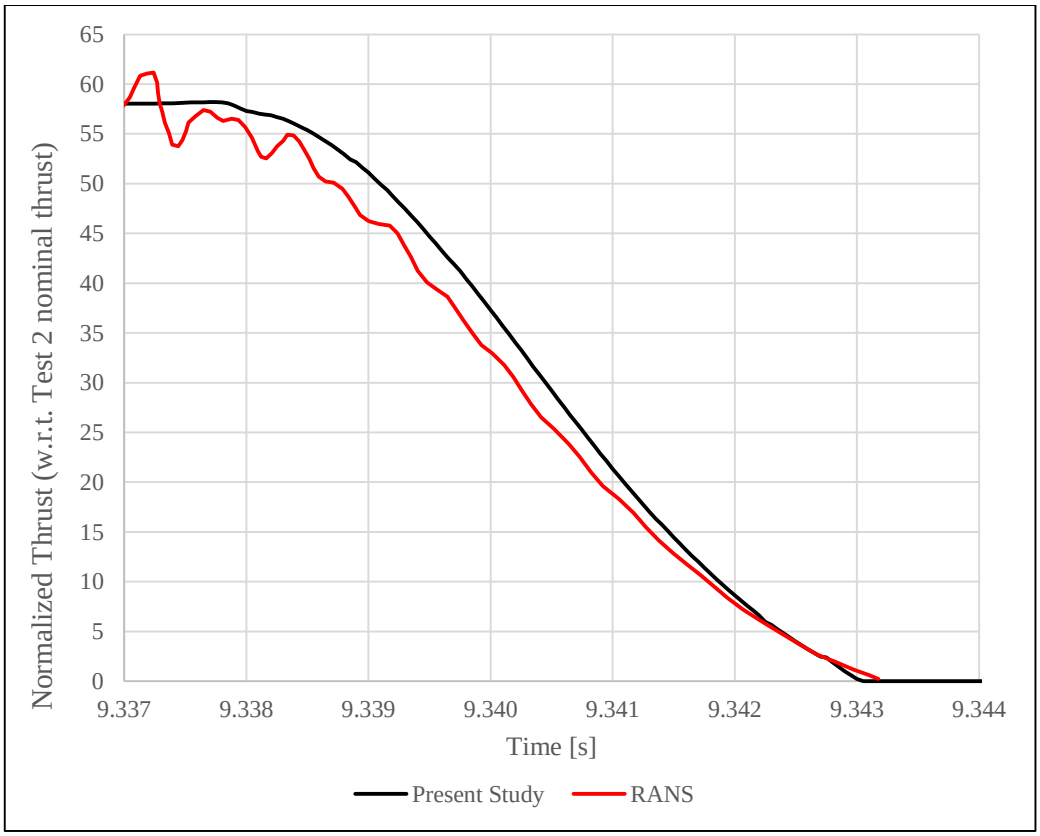

Figure 3.9. Thrust vs. time curve obtained by RANS simulation, compared to the results of the solver (results from the simulation of Test 2)

While the thrust profile cannot be captured by the solver, another important parameter to consider, which is the total impulse at the thrust termination phase, is calculated with an absolute error of 3.8% for Test 1 and 0.6% for Test 2, which is a satisfactory result for the purpose of this study. So, it can be concluded that for the pressure range and the motor geometry under consideration in this validation study, as an integral property the thrust behaves as it is calculated by the solver, but capturing the extremum values of the thrust needs more sophisticated tools.

3.5 Evaluation of the Transient Behavior of the Solution

3.5.1 Evolution of the Temperature Distribution Inside the Propellant Grain During the Rapid Depressurization Phase

The temperature profile of the solid propellant grain, which is calculated at each time step, is plotted for some time instants for a better understanding of the solution evolution. Figure 3.10 illustrates the change in the propellant temperature distribution while the solution proceeds for the simulation of Test 2. In the graph, θ is the non-dimensional temperature, whose value ranges between 0 and 1 as a result of the boundary conditions, and Y is the unitless spatial coordinate inside the 1-D propellant grain, which extends to $-\infty$. The point where Y = 0 represents the propellant surface and Y gets decreased while marching inside the solid. Since $\theta = 0$ at $-\infty$ (It is assumed that T at $-\infty$ remains T_0 for the whole firing interval), the horizontal axis of the graph is limited at a value where θ reaches 0. In the figure, t0 represents the time instant at which the annular channel is opened for the first time, and the other profiles correspond to the instants that are some time after t0.

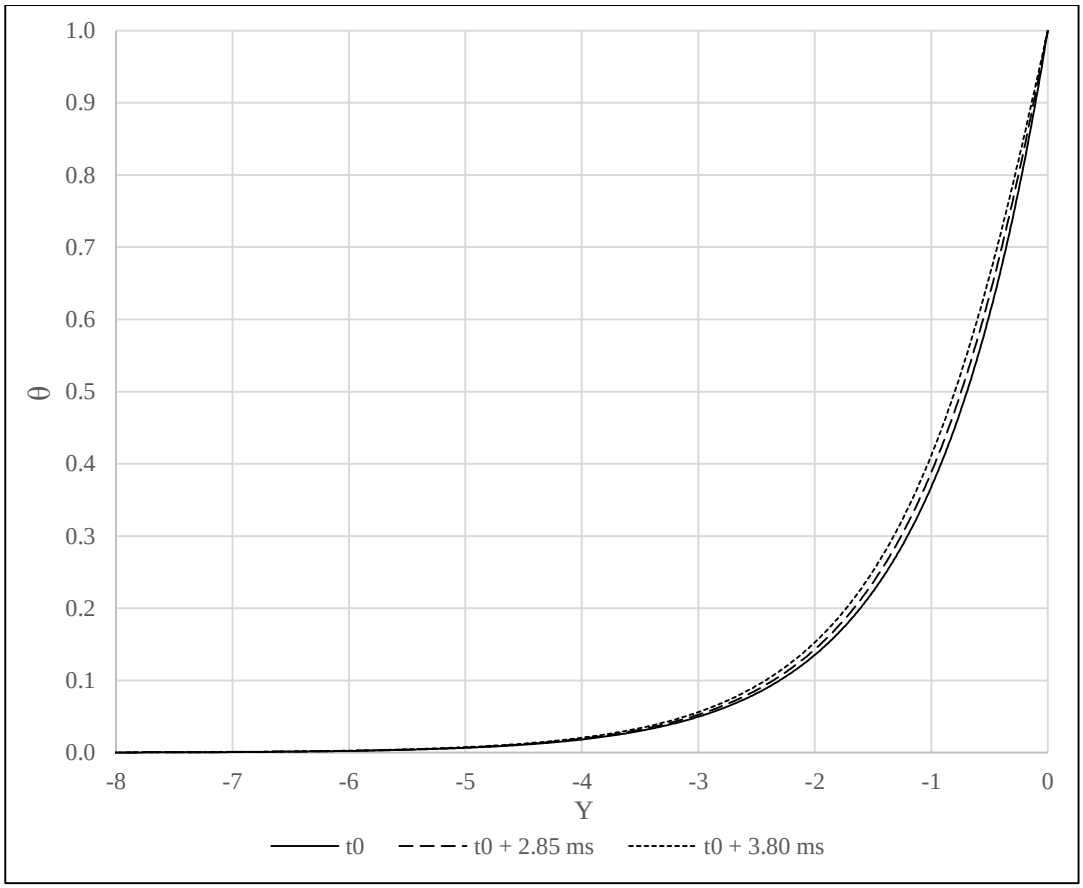

Figure 3.10. Temperature profile inside the propellant grain, at several time instants before extinguishment (results from the simulation of Test 2)

Observing Figure 3.10, it can be deduced that the temperature profile of the solid gets thicker as the time advances. This is due to the chamber pressure and heat transfer to the propellant surface being reduced continuously while the solution proceeds. As the heat transfer to the surface is being reduced, the corresponding burn rate decreases as well. As a result, a lower temperature gradient at the propellant surface is calculated for a lower burn rate case, which means that heat can penetrate further inside the propellant simply because there is more time for heat to penetrate, when compared to a case of higher burn rate. For this reason, the temperature gradient at the surface becomes steeper as the burn rate increases.

3.5.2 Evolution of the Instantaneous Burn Rate During the Rapid Depressurization Phase

The instantaneous propellant burn rate, which is one of the most important outputs of the solution, is plotted for the whole termination interval, and is illustrated in Figure 3.11. The values of the burn rates are non-dimensionalized with respect to the nominal burn rate of the propellant that is calculated during the normal operation of the motor.

The steady burn rate of the propellant is calculated for the entire firing interval and is used for the pressure calculation before the annular channel is formed around the detachable nozzle. After the channel is opened, the unsteady burn rate module is invoked and the instantaneous propellant burn rate starts to being calculated for the pressure calculations. Up to that point, the instantaneous burn rate is taken to be equivalent to the steady state burn rate since there is no drastic changes in the pressure.

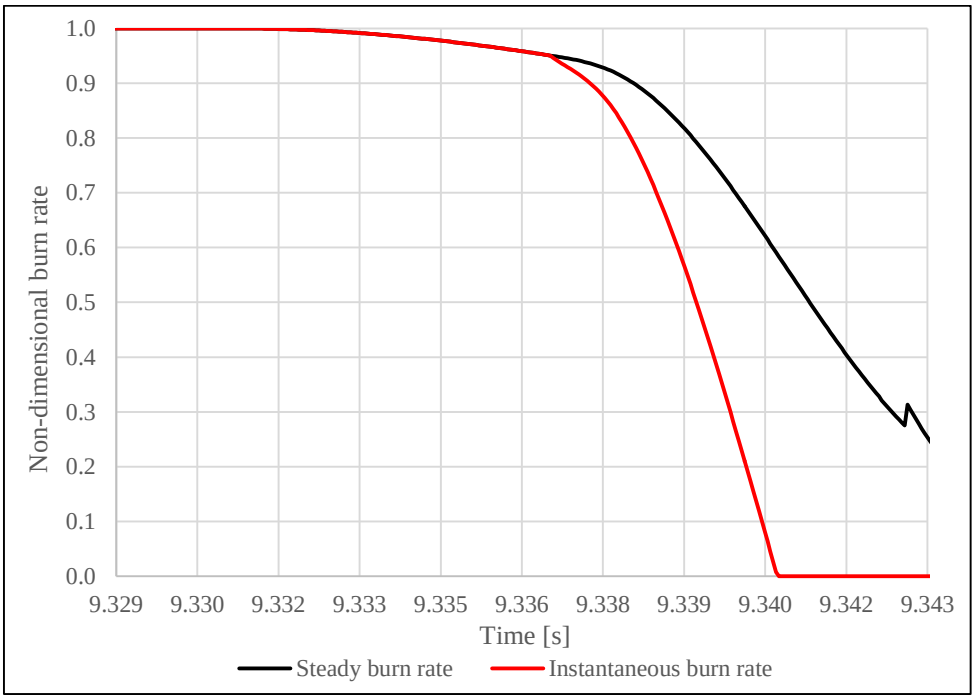

Figure 3.11. Transient profile of the propellant burn rate during termination (results from the simulation of Test 2)

Figure 3.11 shows that the burn rate mildly drops because of the decreasing chamber pressure, caused by increasing internal volume up to the point where the annular channel is opened. When the auxiliary nozzle shows up, unsteady burn rate starts to being calculated where the steep drop in the burn rate starts. From that point forward, the chamber pressure drops drastically, meaning that the heat transfer from the gas phase to the propellant surface decreases significantly at each subsequent time step.

Figure 3.12 illustrates the instantaneous temperature profile of the propellant at a time instant (t = 9.34 s) that is after the initiation of steep pressure drop and before extinguishment. Together with the actual profile (instantaneous temperature profile calculated by the solver), the corresponding steady state temperature profile is also plotted for the purpose of comparing the two profiles. The corresponding steady state temperature profile is the profile that would be obtained inside the propellant at steady state when the heat transfer to the propellant surface equals the heat transfer at t = 9.34 s.

In Figure 3.12, it can be observed that the instantaneous temperature profile is steeper at the surface when compared to the steady state profile. The reason behind the two profiles being quite different is the lag in the heat transfer inside the solid phase with respect to the gas phase. While the heat transfer from the gas phase responds to the pressure changes quickly and reaches its steady-state value almost instantly, heat transfer in the solid phase (propellant) cannot be assumed as a steady-state process because of the characteristic times associated with the gas phase and the solid phase (Hart & McClure, 1959). As a result, the temperature distribution inside the propellant grain cannot reach its steady state as opposed to the gas phase at a time instant in the rapid depressurization phase.

Just before the rapid depressurization, the chamber pressure is at a certain value and the temperature profile of the propellant is at its steady state corresponding to that chamber pressure. Since the pressure drops rapidly after that instant, the instantaneous temperature distribution inside the propellant is still close to its state before depressurization, which has a larger slope at the surface, compared to the

steady temperature profile corresponding to that pressure. This is exactly the case that is illustrated by Figure 3.12 at t = 9.34 s. For the same amount of heat input, larger slope at the surface means a larger portion of the heat energy being spent on heating the solid, compared to the steady profile. This in turn causes less energy being spent on burning the solid, causing the instantaneous burn rate being lower than the steady burn rate corresponding to that pressure, as it can be observed in Figure 3.11. Physically, it means that for an instant in the termination phase, the heat transfer to the surface is not sufficient for the propellant to burn with its steady state burn rate at that pressure, because the temperature profile inside the propellant has not enough time in order to develop, leading to failure in propellant burn and a full extinguishment (burn rate equals zero) at some point.

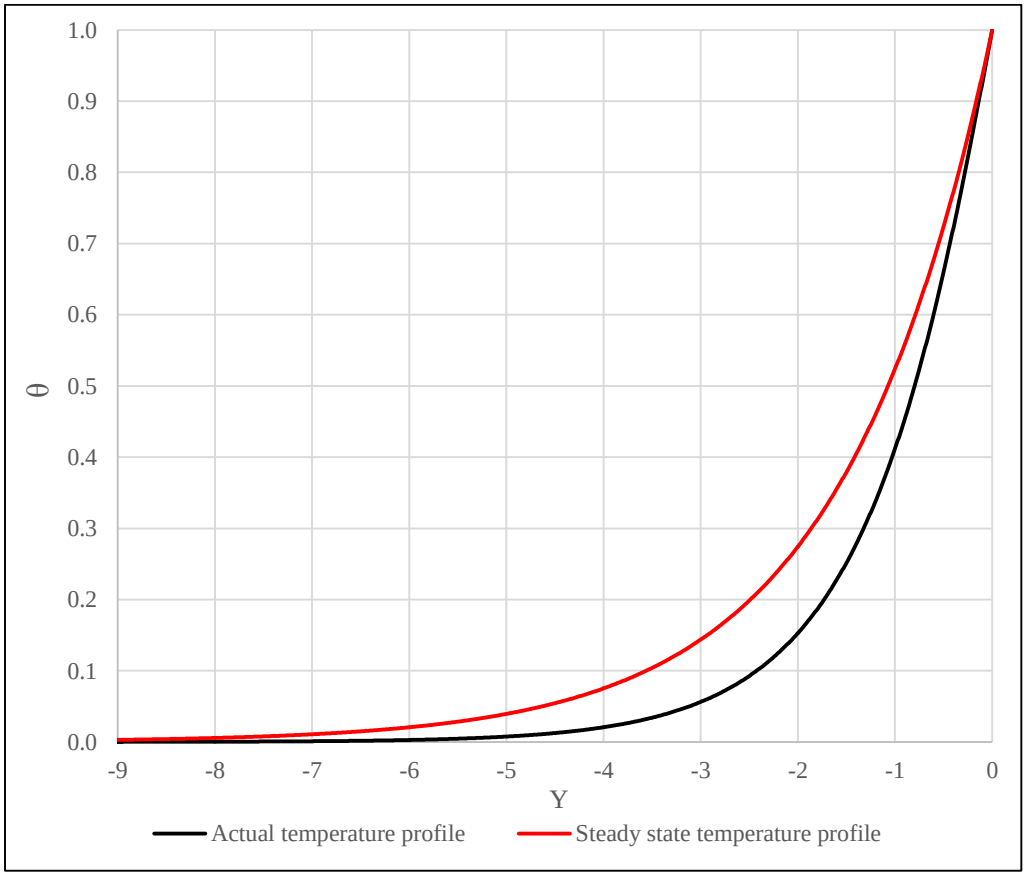

Figure 3.12. Temperature profile of the propellant at t = 9.34 s, plotted together with the steady state temperature profile that would be formed with the heat feedback at the same time instant (results from the simulation of Test 2)

CHAPTER 4

CONCLUDING REMARKS

In order to investigate the feasibility of a solid propellant rocket motor with the extinguishment by nozzle detachment ability and to derive a both cheap and accurate performance estimation method for such a propulsion system, an internal ballistic solver that utilizes a transient burning rate model, which requires a number of propellant and motor properties that are easy to obtain, has been developed. The solver calculates the time history of the performance parameters at both normal operation and thrust termination phases, which serves as a tool for the design of such a system.

For the purpose of validating the ballistic solver, a series of static firings were performed. Propellant extinguishment has been encountered in the firings as it was estimated by the solver, confirming that a solid rocket motor with a shut down ability is possible. Comparing both firings to the results of the solver, a satisfactory agreement has been achieved especially between the pressure vs. time curves produced by the firings and the solver. In addition, decrease in the termination time at a higher operating pressure, which was estimated by the solver, has also been observed experimentally.

The thrust measurements obtained from the static firings and the results of the thrust calculations suggest that the elastic response of the motor may play an important role in the thrust output after termination. Regardless of the termination method, if a load carrying part is seperated from the motor at one point, the effect of a sudden change in the force balance of the structure needs to be accounted for if the transient behavior of the thrust output is a design parameter of interest, which is often the case in the design of solid rocket motors.

While the thrust profile at the termination phase could not be captured, the total impulse has been estimated with a satisfactory accuracy. In order to estimate the peaks and valleys at the thrust history, a spring-mass-damper solver is planned to be added as a future work. However, considering the overall performance, with these abilities and limitations in mind, the developed method in this study can be used as a practical solution for the extinguishment problem.

REFERENCES

Ansys® Enterprise Fluent, Release 20.1, Fluent User Guide, ANSYS, Inc.

Cohen, N. S., Fleming, R. W., & Derr, R. L. (1974). Role of binders in solid propellant combustion. AIAA Journal, 12(2), 212–218. https://doi.org/10.2514/3.49195

Greatrix, D. R. (2008). Transient burning rate model for solid rocket motor internal ballistic simulations. International Journal of Aerospace Engineering, 2008, 1–10. https://doi.org/10.1155/2008/826070

Guirao, C., & Williams, F. A. (1971). A model of ammonium perchlorate deflagration between 20 and 100 ATM. AIAA Journal, 9(7), 1345–1356. https://doi.org/10.2514/3.6355

Hart, R. W., & McClure, F. T. (1959). Combustion instability: Acoustic interaction with a burning propellant surface. The Journal of Chemical Physics, 30(6), 1501–1514. https://doi.org/10.1063/1.1730226

Horton, M. D., Bruno, P. S., & Graesser, E. C. (1968). Depressurization induced extinction of burning solid propellant. AIAA Journal, 6(2), 292–297. https://doi.org/10.2514/3.4492

Keenan, A. G., & Siegmund, R. F. (1968). The thermal decomposition of ammonium perchlorate: A literature review. https://doi.org/10.21236/ad0673542

Kumar, V. R. (2007). Evaluation of dynamic burn rate from the extinction compliance of solid rocket motors. Journal of Spacecraft and Rockets, 44(2), 453–456. https://doi.org/10.2514/1.20424

Lenoir, J. M., & Robillard, G. (1957). A mathematical method to predict the effects of erosive burning in solid-propellant rockets. Symposium (International) on Combustion, 6(1), 663–667. https://doi.org/10.1016/s0082-0784(57)80092-7

Summerfield, M., Caveny, L. H., Battista, R. A., Kubota, N., Gostintsev, Y. U. A., & Isoda, H. (1971). Theory of dynamic extinguishment of solid propellants with special reference to nonsteady heat feedback law. Journal of Spacecraft and Rockets, 8(3), 251–258. https://doi.org/10.2514/3.30256

Sutton, G. P., & Biblarz, O. (2017). Rocket Propulsion Elements. John Wiley & Sons Inc.

Taback, H. J., Day, E. E., & Browne, T. P. (1965). Combustion termination of solid rocket motors. Journal of Spacecraft and Rockets, 2(3), 332–337. https://doi.org/10.2514/3.28180

Turk, S. L., Battista, R. A., Kuo, K. K., Caveny, L. H., & Summerfield, M. (1973). Dynamic responses of solid rockets during rapid pressure change. Journal of Spacecraft and Rockets, 10(2), 137–142. https://doi.org/10.2514/3.61859